J|A|C|S
ARTICLES
Published on Web 04/08/2004

Strategy for the Study of Paramagnetic Proteins with Slow Electronic Relaxation Rates by NMR Spectroscopy: Application to Oxidized Human [2Fe-2S] Ferredoxin†

Timothy E. Machonkin, William M. Westler, and John L. Markley*

Contribution from the National Magnetic Resonance Facility at Madison, Department of Biochemistry, University of Wisconsin−Madison, Madison, Wisconsin 53706

Received July 4, 2003; E-mail: markley@nmrfam.wisc.edu

Abstract: NMR studies of paramagnetic proteins are hampered by the rapid relaxation of nuclei near the paramagnetic center, which prevents the application of conventional methods to investigations of the most interesting regions of such molecules. This problem is particularly acute in systems with slow electronic relaxation rates. We present a strategy that can be used with a protein with slow electronic relaxation to identify and assign resonances from nuclei near the paramagnetic center. Oxidized human [2Fe-2S] ferredoxin (adrenodoxin) was used to test the approach. The strategy involves six steps: (1) NMR signals from ^{1}H, ^{13}C, and ^{15}N nuclei unaffected or minimally affected by paramagnetic effects are assigned by standard multinuclear two- and three-dimensional (2D and 3D) spectroscopic methods with protein samples labeled uniformly with ^{13}C and ^{15}N. (2) The very broad, hyperfine-shifted signals from carbons in the residues that ligate the metal center are classified by amino acid and atom type by selective ^{13}C labeling and one-dimensional (1D) ^{13}C NMR spectroscopy. (3) Spin systems involving carbons near the paramagnetic center that are broadened but not hyperfine-shifted are elucidated by ^{13}C{^{13}C} constant time correlation spectroscopy (CT-COSY). (4) Signals from amide nitrogens affected by the paramagnetic center are assigned to amino acid type by selective ^{15}N labeling and 1D ^{15}N NMR spectroscopy. (5) Sequence-specific assignments of these carbon and nitrogen signals are determined by 1D ^{13}C{^{15}N} difference decoupling experiments. (6) Signals from ^{1}H nuclei in these spin systems are assigned by paramagnetic-optimized 2D and 3D ^{1}H{^{13}C} experiments. For oxidized human ferredoxin, this strategy led to assignments (to amino acid and atom type) for 88% of the carbons in the [2Fe-2S] cluster-binding loops (residues 43−58 and 89−94). These included complete carbon spin-system assignments for eight of the 22 residues and partial assignments for each of the others. Sequence-specific assignments were determined for the backbone ^{15}N signals from nine of the 22 residues and ambiguous assignments for five of the others.

1. Introduction

NMR Spectroscopy of Paramagnetic Proteins. NMR has proven to be a powerful tool in the study of paramagnetic proteins.[1−9] Hyperfine-shifted NMR signals, which report on the delocalization of unpaired spin density from iron atoms onto nuclei of the protein, have been particularly useful for obtaining insight into the geometric and electronic structure of the paramagnetic center. For example, hyperfine data have contributed to our understanding of the electronic coupling among metal centers in plant [2Fe-2S] ferredoxins[10] and in various [4Fe-4S] proteins,[11,12] and they have been used to probe hydrogen-bond lengths in rubredoxin.[13−15]

Paramagnetic systems with fast electronic relaxation rates, such as heme proteins and [4Fe-4S] proteins, are amenable to two- and three-dimensional (2D and 3D) methods. In such systems electron−nuclear interactions readily provide geometric constraints, including the electron−nuclear dipolar contribution to T_1 relaxation rates,[16,17] pseudocontact shifts,[18,19] and residual

† NMR chemical shifts have been deposited at BioMagResBank under bmr 6026.

(1) Bertini, I.; Luchinat, C. *NMR of Paramagnetic Molecules in Biological System*; Benjamin/Cummings: Menlo Park, CA, 1986.
(2) Bertini, I.; Turano, P.; Vila, A. J. *Chem. Rev.* **1993**, *93*, 2833−2932.
(3) Cheng, H.; Markley, J. L. *Annu. Rev. Biophys. Biomol. Struct.* **1995**, *24*, 209−237.
(4) Bertini, I.; Luchinat, C.; Rosato, A. *Prog. Biophys. Mol. Biol.* **1996**, *66*, 43−80.
(5) Bertini, I.; Luchinat, C.; Rosato, A. *Adv. Inorg. Chem.* **1999**, *47*, 251−282.
(6) Goodfellow, B. J.; Macedo, A. L. *Annu. Rep. NMR Spectrosc.* **1999**, *37*, 119−177.
(7) Bertini, I.; Luchinat, C.; Piccioli, M. *Methods Enzymol.* **2001**, *339*, 314−340.
(8) Bertini, I.; Luchinat, C.; Parigi, G. *Solution NMR of Paramagnetic Molecules*; Elsevier: Amsterdam, 2001.
(9) Machonkin, T. E.; Markley, J. L. In *Encyclopedia of Nuclear Magnetic Resonance*; Grant, D. M., Harris, R. K., Eds.; Wiley: Chichester, U.K., 2002; Vol. 9, pp 384−401.
(10) Dugad, L. B.; La Mar, G. N.; Banci, L.; Bertini, I. *Biochemistry* **1990**, *29*, 2263−2271.
(11) Banci, L.; Bertini, I.; Ciurli, S.; Ferretti, S.; Luchinat, C.; Piccioli, M. *Biochemistry* **1993**, *32*, 9387−9397.
(12) Bertini, I.; Briganti, F.; Luchinat, C.; Messori, L.; Monnanni, R.; Scozzafava, A. *Eur. J. Biochem.* **1992**, *204*, 831−839.
(13) Xia, B.; Westler, W. M.; Cheng, H.; Meyer, J.; Moulis, J.-M.; Markley, J. L. *J. Am. Chem. Soc.* **1995**, *117*, 5347−5350.
(14) Wilkens, S. J.; Xia, B.; Weinhold, F.; Markley, J. L.; Westler, W. M. *J. Am. Chem. Soc.* **1998**, *120*, 4806−4814.
(15) Lin, I.-J.; Gebel, E. B.; Machonkin, T. E.; Westler, W. M.; Markley, J. L. *J. Am. Chem. Soc.* **2003**, *125*, 1464−1465.
(16) Huber, J. G.; Moulis, J.-M.; Gaillard, J. *Biochemistry* **1996**, *35*, 12705−12711.

dipolar couplings by magnetic alignment.[20,21] Excellent discussions of these types of constraints and their relative merits are available.[22,23]

The more challenging paramagnetic proteins for NMR spectroscopy are ones with slow electronic relaxation rates, such as the [2Fe-2S] proteins discussed here. In these systems, the nuclei close to the paramagnetic center frequently relax too rapidly to be studied by conventional 2D and 3D NMR techniques. Thus, what usually is the most interesting part of the protein is unobservable by these approaches. In many such cases, the hyperfine shifts of nuclei located near the metal center are sufficiently large that the signals can be resolved by one-dimensional (1D) NMR, despite their large line widths. This is frequently true for nuclei with lower magnetogyric ratios (e.g., ^{15}N, ^{13}C, and ^{2}H), whose signals are broadened less than ^{1}H. One-dimensional NMR approaches, however, do not provide the connectivity information needed for assignments. More difficult to resolve are signals from nuclei that are close in space to the metal center but separated from it by several chemical bonds: such resonances may be severely broadened by electron−nuclear dipolar relaxation and obscured by the slowly relaxing diamagnetic signals from the rest of the protein, which they overlap because they do not have appreciable hyperfine shifts.

Newer NMR Approaches. Directly detected ^{13}C NMR offers advantages for the study of the more difficult types of paramagnetic centers in proteins. Because the three contributions to paramagnetic relaxation (dipolar, Curie, and contact) are each proportional to $1/\gamma_N^2$, ^{13}C offers as much as a 16-fold improvement in line width compared to ^{1}H. In earlier studies of oxidized *Anabaena* PCC7120 vegetative [2Fe-2S] ferredoxin, we have exploited 1D ^{13}C NMR methods to resolve signals,[24,25] the heteronuclear difference decoupling experiment of Redfield and co-workers[26] to identify the connectivity between Cys46 C′ and Ala45 N in a sample labeled selectively with [^{15}N]Cys and [^{13}C′]-Ala,[25] and 2D ^{13}C{^{13}C} NMR to assign residues distant from the paramagnetic center (diamagnetic region).[27,28] We recently demonstrated the use of 2D ^{13}C{^{13}C} constant time correlation spectroscopy (CT-COSY) for obtaining connectivity information in the cluster-binding loops of oxidized human [2Fe-2S] Fd ($HuFd_{ox}$, also called adrenodoxin).[29]

Others have developed similar approaches. Pochapsky and co-workers employed selective double labeling and ^{13}C{^{15}N} 1D difference decoupling to obtain extensive backbone assignments for the loops ligating the paramagnetic metal cluster in oxidized and reduced *Pseudomonas putida* [2Fe-2S] Fd (putidaredoxin).[30−33] Bertini and co-workers used regular ^{13}C{^{13}C} COSY to obtain connectivity information between the carbonyls ligating the metal center and the aliphatic carbons in Ce(III)-substituted calbindin D9k[34] and then utilized these data as constraints in the solution structure determination.[22] Pochapsky and co-workers demonstrated the use of ^{13}C{^{13}C} homonuclear and ^{13}C{^{15}N} heteronuclear multiple quantum correlation spectroscopy to obtain backbone connectivity information in a Ni(II)-containing protein.[35]

NMR Spectroscopy of Ferredoxins. Ferredoxins (Fds) may be broadly classified into three types: plant-type, vertebrate-type, and clostridial-type. Clostridial-type Fds are dramatically different from the other two.[36] Plant- and vertebrate-type Fds exhibit considerable sequence identity within each class and limited identity between classes.[37] Structures have been determined by X-ray crystallography for representatives of each type in the oxidized state.[38,39] Note that there are no crystal structures reported for any reduced [2Fe-2S] cluster, either in a protein or for a synthetic model complex.[40] The metrical parameters of the [2Fe-2S] cluster are essentially identical in both plant- and vertebrate-type ferredoxins in the oxidized state, with the exception of the dihedral angles of one Cys side chain (compare, for example, Morales et al.[38] and Müller et al.[39]). However, reduced plant- and vertebrate-type ferredoxins exhibit very different electronic structures as evidenced by electron paramagnetic resonance (EPR) and Mössbauer spectra and other physical properties.[41−44] Vertebrate-type Fds also exhibit a structural feature unusual for an electron-transfer protein: a conformational change upon reduction, as shown definitively through comparison of the ^{13}C and ^{15}N backbone resonances of the diamagnetic region of HuFd in both oxidation states.[45] Major changes in chemical shift upon reduction were found in residues 29−32 and 109−114, and smaller changes in residues

(17) Bertini, I.; Donaire, A.; Luchinat, C.; Rosato, A. *Proteins: Struct., Funct., Genet.* **1997**, *29*, 348−358.
(18) Harper, L. V.; Amann, B. T.; Vinson, V. K.; Berg, J. M. *J. Am. Chem. Soc.* **1993**, *115*, 2577−2580.
(19) Banci, L.; Bertini, I.; Savellini, G. G.; Romagnoli, A.; Turano, P.; Cremonini, M. A.; Luchinat, C.; Gray, H. B. *Proteins: Struct., Funct., Genet.* **1997**, *29*, 68−76.
(20) Tolman, J. R.; Flanagan, J. M.; Kennedy, M. A.; Prestegard, J. H. *Proc. Natl. Acad. Sci. U.S.A.* **1995**, *92*, 9279−9283.
(21) Banci, L.; Bertini, I.; Huber, J. G.; Luchinat, C.; Rosato, A. *J. Am. Chem. Soc.* **1998**, *120*, 12903−12909.
(22) Bertini, I.; Donaire, A.; Jiménez, B.; Luchinat, C.; Parigi, G. *J. Biomol. NMR* **2001**, *21*, 85−98.
(23) Bertini, I.; Luchinat, C.; Parigi, G. *Concepts Magn. Reson.* **2002**, *14*, 259−286.
(24) Chan, T.-M.; Markley, J. L. *Biochemistry* **1983**, *22*, 6008−6010.
(25) Cheng, H.; Westler, W. M.; Xia, B.; Oh, B.-H.; Markley, J. L. *Arch. Biochem. Biophys.* **1995**, *316*, 619−634.
(26) Weiss, M. A.; Redfield, A. G.; Griffey, R. H. *Proc. Natl. Acad. Sci. U.S.A.* **1986**, *83*, 1325−1329.
(27) Oh, B. H.; Westler, W. M.; Darba, P.; Markley, J. L. *Science* **1988**, *240*, 908−911.
(28) Oh, B.-H.; Mooberry, E. S.; Markley, J. L. *Biochemistry* **1990**, *29*, 4004−4011.
(29) Machonkin, T. E.; Westler, W. M.; Markley, J. L. *J. Am. Chem. Soc.* **2002**, *124*, 3204−3205.
(30) Jain, N. U.; Pochapsky, T. C. *J. Am. Chem. Soc.* **1998**, *120*, 12984−12985.
(31) Jain, N. U.; Pochapsky, T. C. *Biochem. Biophys. Res. Commun.* **1999**, *258*, 54−59.
(32) Jain, N. U. *NMR Study of the Active Site in Putidaredoxin, An Electron-Transfer Protein*; Brandeis University, 2000.
(33) Pochapsky, T. C.; Kostic, M.; Jain, N.; Pejchal, R. *Biochemistry* **2001**, *40*, 5602−5614.
(34) Bertini, I.; Lee, Y.-M.; Luchinat, C.; Piccioli, M.; Poggi, L. *ChemBioChem* **2001**, *2*, 550−558.
(35) Kostic, M.; Pochapsky, S. S.; Pochapsky, T. C. *J. Am. Chem. Soc.* **2002**, *124*, 9054−9055.
(36) Meyer, J. *FEBS Lett.* **2001**, *509*, 1−5.
(37) Bertini, I.; Luchinat, C.; Provenzani, A.; Rosato, A.; Vasos, P. R. *Proteins: Struct., Funct., Genet.* **2002**, *46*, 110−127.
(38) Morales, R.; Chron, M.-H.; Hudry-Clergeon, G.; Pétillot, Y.; Norager, S.; Medina, M.; Frey, M. *Biochemistry* **1999**, *38*, 15764−15773.
(39) Müller, A.; Müller, J. J.; Muller, Y. A.; Uhlmann, H.; Berhardt, R.; Heinemann, U. *Structure* **1998**, *6*, 269−280.
(40) Morales et al. claim to have reported the structure of reduced *Anabaena* Fd; however, they admit that their sample was a mixture of oxidized and reduced and offer no evidence to quantitate the amounts. Notably, the bond Fe−S bond lengths they report do not change upon reduction. Thus, their structure cannot rightly be considered to be that of a reduced Fd. EXAFS studies of [2Fe-2S] Fds have shown increases in both the Fe−Fe and average Fe−S distances upon reduction (Teo, B.-T.; Shulman, R. G.; Brown, G. S., Meixner, A. E. *J. Am. Chem. Soc.* **1979**, *101*, 5642−5631, and Cosper, N. J.; Cosper, M. M.; Johnson, M. L.; Iwasaki, T.; Meyer, J.; Scott, R. A. *J. Inorg. Biochem.* **2001**, *86*, 187); however, it is not possible to ascertain what impact that might have on the structure of the rest of the protein.
(41) Bertrand, P.; Gayda, J.-P. *Biochim. Biophys. Acta* **1979**, *579*, 107−121.
(42) Sands, R. H.; Dunham, W. R. *Q. Rev. Biophys.* **1975**, *7*, 443−504.
(43) Guigliarelli, B.; Bertrand, P. *Adv. Inorg. Chem.* **1999**, *47*, 421−497.
(44) Fu, W.; Drozdzewski, P. M.; Davies, M. D.; Sligar, S. G.; Johnson, M. K. *J. Biol. Chem.* **1992**, *267*, 15502−15510.
(45) Xia, B.; Volkman, B. F.; Markley, J. L. *Biochemistry* **1998**, *37*, 3965−3973.

78−82. Signals from residues 109−124, which were not resolved in spectra of oxidized HuFd, were observed and assigned in spectra of the reduced protein. This suggested that the C-terminus is flexible in $HuFd_{ox}$ but becomes ordered in $HuFd_{red}$.

A number of NMR solution structures have now been reported for [2Fe-2S] Fds. Four solution structures are available for plant-type Fds: three in the oxidized state (*Synechocystis* PCC6803,[46] *Synechococcus elongatus*,[47,48] and parsley[49]), and one in the reduced state for the *Methylcoccus capsulatus* soluble methane monooxygenase reductase ferredoxin domain (MMOR-Fd),[50] which is in the plant-type class as determined by sequence homology and spectroscopy.[51] Four solution structures are also available for vertebrate-type Fds: putidaredoxin (Pd_{ox})[52,53] and terpredoxin[54] from *Pseudomonas* (both in the oxidized state) and bovine Fd (BoFd) in each of its accessible redox states.[55,56] In the NMR studies leading to the *Synechocystis*, *S. elongatus*, MMOR-Fd, Pd_{ox}, and terpredoxin structures, signals were not detected from a number of residues (13 and 21, depending on the protein) near the [2Fe-2S] cluster. The [2Fe-2S] cluster regions were modeled on the basis of crystallographic data from other Fds (at least 32 constraints), and either no[48,50,53] or very few[46,47,52,54] paramagnetic NMR constraints were used. These constraints were distance estimates inferred from the absence of signals that were presumed to be broadened beyond detection by paramagnetic relaxation. In the spectra used to determine the parsley Fd structure, some signals from nuclei near the [2Fe-2S] cluster were assigned by $^1H\{^1H\}$ 2D NMR; still, signals from nine residues could not be detected, and those from another five had incomplete assignments. A limited number (33) of paramagnetic ^1H T_1 values were used as constraints, although none closer than two residues from the Cys ligands, and more limited constraints derived from crystallographic data were imposed for the [2Fe-2S] cluster and Cys ligands (18). This resulted in the best solution structure yet available (backbone root-mean-square deviation for the family of 18 structures of 0.52 Å). In the data used in determining the structures of oxidized and reduced BoFd, signals from 19 and 25 residues, respectively, were not detected. Both crystallographic data and paramagnetic ^1H T_1 values were used to develop the geometric model of the [2Fe-2S] cluster, although the details were not given.[56] Unlike in plant-type Fds,[10,25,57] the electronic relaxation rate in vertebrate-type Fds is *slower* in the reduced state than in the oxidized state. Signals from nuclei near the [2Fe-2S] cluster of reduced vertebrate-type Fds[30,58−60] are broadened more severely than in oxidized. This explains the larger number of residues whose signals were undetected in reduced versus oxidized BoFd and the difference in the backbone root-mean-square deviations for the annealed structures (1.53 for reduced BoFd vs 0.94 Å for oxidized BoFd).

Previous Work on Vertebrate Ferredoxins. Earlier work from this laboratory on $HuFd_{ox}$ led to assignments for the diamagnetic region of the protein backbone (H^N, N, H^α, C^α, C′) and the C^β carbons. These were obtained by traditional ^1H-detected 2D and 3D NMR experiments.[45] Signals from residues 1, 44−58, 90−93, 107, and 115−124 were not detected, and assignments for residues 2, 28−31, 43, 85, 87−88, 94, 105−106, and 114 were incomplete. Partial side-chain assignments for H10, H56, and H62 were obtained by ^1H-detected 1D and 2D NMR experiments.[61] The lack of assignments to residues 114−124, which are known to be highly dynamic, may be the result of exchange broadening (note that the backbone assignments relied heavily upon detection of the H^N); residues 105−107 also may be affected by dynamics. Residues 30 and 31 are close to the [2Fe-2S] cluster (the crystal structure of truncated $BoFd_{ox}$[40] shows that H^α of L30 is 7.77 Å from the Fe−Fe midpoint).

Other groups have used analogous methods to assign spectra of nearly identical iron−sulfur proteins: Pochapsky and co-workers for a truncated form of $HuFd_{ox}$ (residues 4−114)[62] and Rüterjans and co-workers for full-length $BoFd_{ox}$.[55,56] In each of those investigations, signals from residues 44−55 and 90−93 were not detected and assignments to residues 43, 57, 89, and 94 were incomplete. Partial assignments to residue 56 were reported only for truncated $HuFd_{ox}$.

The Cys ligands to the cluster are C46, C52, C55, and C92. Residues 43−58 and 89−94, designated here as the cluster-binding loops, thus are expected to be those most affected by paramagnetic broadening from the [2Fe-2S] cluster. As summarized below, previous studies utilizing traditional diamagnetic NMR methods have yielded few assignments to resonances from the cluster-binding loop residues. These earlier investigations include ours on $HuFd_{ox}$,[45] the work of Pochapsky and co-workers on truncated $HuFd_{ox}$,[62] and the investigations of Rüterjans and co-workers on $BoFd_{ox}$.[55,56]

(1) F43. Assignments reported for this residue include the $^1H^N$, $^1H^\alpha$, ^{15}N, $^{13}C^\alpha$, and $^{13}C^\beta$ resonances of $HuFd_{ox}$;[45] the $^1H^\beta$, ring proton, and $^{13}C^\delta$ resonances of truncated $HuFd_{ox}$;[62] and the $^1H^\beta$ and $^{13}C'$ resonances of $BoFd_{ox}$.[55,56] These cover all resonances with the exception of the remaining ring carbons.

(2) H56. Assignments for this residue include the $^1H^{\epsilon 1}$, $^1H^{\delta 2}$, $^{15}N^{\epsilon 2}$, $^{15}N^{\delta 1}$, $^{13}C^{\epsilon 1}$, and $^{13}C^{\delta 2}$ resonances of $HuFd_{ox}$[45] and the $^1H^{\delta 1}$ resonce of truncated $HuFd_{ox}$.[62] Lacking are assignments to the backbone nuclei and the side-chain $^1H^{\beta 2}$, $^1H^{\beta 3}$, and $^{13}C^\beta$ nuclei.

(3) L57. Assignments for this residue in truncated $HuFd_{ox}$ are complete with the exception of $^1H^{\delta 2}$ and $^{13}C^{\delta 2}$.[62] Assignments in $BoFd_{ox}$ are somewhat less complete.[55,56]

(46) Lelong, C.; Sétif, P.; Bottin, H.; André, F.; Neumann, J.-M. *Biochemistry* **1995**, *34*, 14462−14473.
(47) Baumann, B.; Sticht, H.; Schärpf, M.; Sutter, M.; Haehnel, W.; Rösch, P. *Biochemistry* **1996**, *35*, 12831−12841.
(48) Hatanaka, H.; Tanimura, R.; Katoh, S.; Inagaki, F. *J. Mol. Biol.* **1997**, *268*, 922−933.
(49) Im, S.-c.; Liu, G.; Luchinat, C.; Sykes, A. G.; Bertini, I. *Eur. J. Biochem.* **1998**, *258*, 465−477.
(50) Müller, J.; Lugovsky, A. A.; Wagner, G.; Lippard, S. J. *Biochemistry* **2002**, *41*, 42−51.
(51) Colby, J.; Dalton, H. *Biochem. J.* **1979**, *177*, 903−908.
(52) Pochapsky, T. C.; Ye, X. M.; Ratnaswamy, G.; Lyons, T. A. *Biochemistry* **1994**, *33*, 6424−6432.
(53) Pochapsky, T. C.; Jain, N. U.; Kuti, M.; Lyons, T. A.; Heymont, J. *Biochemistry* **1999**, *38*, 4681−4690.
(54) Mo, H.; Pochapsky, S. S.; Pochapsky, T. C. *Biochemistry* **1999**, *38*, 5666−5675.
(55) Weiss, R.; Brachais, L.; Löhr, F.; Hartleib, J.; Bernhardt, R.; Rüterjans, H. *J. Biomol. NMR* **2000**, *17*, 355−356.
(56) Beilke, D.; Weiss, R.; Löhr, F.; Pristovsek, P.; Hannemann, F.; Bernhardt, R.; Rüterjans, H. *Biochemistry* **2002**, *41*, 7969−7978.
(57) Skjeldal, L.; Westler, W. M.; Oh, B.-H.; Krezel, A. M.; Holden, H. M.; Jacobson, B. L.; Rayment, I.; Markley, J. L. *Biochemistry* **1991**, *30*, 7363−7368.
(58) Ratnaswamy, G.; Pochapsky, T. C. *J. Magn. Reson.* **1993**, *31*, S73−S77.
(59) Sari, N.; Holden, M. J.; Mayhew, M. P.; Vilker, V. L.; Coxon, B. *Biochem. Biophys. Res. Commun.* **1998**, *249*, 773−780.
(60) Xia, B.; Jenks, D.; LeMaster, D. M.; Westler, W. M.; Markley, J. L. *Arch. Biochem. Biophys.* **2000**, *373*, 328−334.
(61) Xia, B.; Cheng, H.; Skjeldal, L.; Coghlan, V.; Vickery, L. E.; Markley, J. L. *Biochemistry* **1995**, *34*, 180−187.
(62) Kostic, M.; Pochapsky, S. S.; Obenauer, J.; Mo, H.; Pagani, G. M.; Pejchal, R.; Pochapsky, T. C. *Biochemistry* **2002**, *41*, 5978−5989.

(4) R89. Assignments for this residue include the backbone resonances with the exception of $^{13}C'$ in $HuFd_{ox}$ [45] and truncated $HuFd_{ox}$.[62] Complete backbone resonances plus those for $^{1}H^{\beta}$ and $^{15}C^{\beta}$ are available for R89 of $BoFd_{ox}$.[55,56]

(5) I94. Assignments for this residue include the $^{13}C^{\alpha}$, $^{13}C'$, $^{13}C^{\beta}$, and $^{1}H^{\alpha}$ resonances for $HuFd_{ox}$[45] and truncated $HuFd_{ox}$[62] and the $^{13}C^{\gamma 1}$, $^{13}C^{\gamma 2}$, and $^{13}C^{\delta 1}$ resonances for $BoFd_{ox}$.[55,56]

(6) Cys Ligands. The 1D ^{1}H spectrum of $HuFd_{ox}$[63] contains a broad unresolved envelope of bands at 24−42 ppm and a single ^{1}H resonance of one proton intensity at 13 ppm. These signals were assigned, respectively, by selective ^{2}H labeling and 1D ^{2}H NMR to Cys $^{1}H^{\beta 2/\beta 3}$ and Cys $^{1}H^{\alpha}$.[60]

Although these approaches led to assignments of a few signals, they failed to yield signals from 12 of the residues in the cluster-binding loops: three Gly (G44, G48, and G91), two Ala (A45 and A51), two Thr (T49 and T54), two Leu (L50 and L90), one Glu (E47), one Ser (S53), and one Gln (Q93). The Cys hydrogen resonances proved to be relatively uninformative because they were overlapped. The structure and electronic properties of the cluster-binding loops are the keys to understanding the electron-transfer properties of this and other proteins. Thus it is clear that new methods are needed for resolving and assigning signals from residues of this class of iron−sulfur protein.

Aims of the Present Work. Our long-term goal has been to develop NMR methodology that is applicable to paramagnetic systems with slow electronic relaxation rates and to bring these tools to bear on several classes of [2Fe-2S] proteins in order to understand the structural origin of their diverse spectroscopic and functional properties. Here, we describe the use of a suite of 1D, 2D, and 3D NMR experiments that are optimized for paramagnetic systems. The centerpiece of this methodology is the 2D $^{13}C\{^{13}C\}$ CT-COSY experiment,[29] although ^{15}N- and ^{1}H-detected experiments are employed as well. We show how this methodology was used to obtain extensive assignments for NMR signals from amino acid residues in the loops that bind the [2Fe-2S] cluster of $HuFd_{ox}$. Finally, we indicate how these results can be used to obtain geometric constraints of the kind that should lead to more meaningful solution structures.

2. Materials and Methods

Chemicals, Bacterial Strains, and Vectors. $^{15}NH_4Cl$, 99% [U-^{13}C]-D-glucose, 99.8% and "100%" D_2O, >95% [^{15}N]-L-alanine, >98% [^{15}N]-L-leucine, 99% [$^{15}C^{\beta}$]-L-cysteine, and sodium 2,2-dimethyl-2-silapentane-5-sulfonate (DSS) were purchased from Cambridge Isotope Laboratories (Andover, MA). [^{15}N,U-^{13}C]-L-cysteine and [^{15}N]-L-threonine (both >98%) were purchased from Martek (now Spectra Stable Isotopes; Columbia, MD). [^{15}N]Glycine (99%) was purchased from Icon (Summit, NJ). Protease inhibitor cocktails were purchased from Calbiochem (San Diego, CA; product number 539137) and Sigma (St. Louis, MO; product number P8340). Isopropyl β-D-thiogalactoside (IPTG) was purchased from LabScientific (Livingston, NJ). Water for NMR samples was purified to a resistivity of >15 MΩ cm^{-1} with an Elga Maxima water purifier (Elga, Inc; Topsfield, MA). All other chemicals were reagent-grade. *Escherichia coli* strain BL21(DE3)/pLysS and the pET9a expression vector were purchased from Novagen (Madison, WI).

Protein Expression and Labeling. The cDNA encoding HuFd was cloned into expression vector pET9a,[45,64] and [U-^{13}C,^{15}N]-HuFd was produced in M9 medium as described previously,[45] with the exception that ~100 μM $FeCl_3$ and 50 mg/L thiamin were added to the medium. For selective labeling, we used synthetic rich (SR) medium, which contains the single isotopically labeled amino acid to be inserted plus high concentrations the other 19 amino acids at natural abundance.[25,65] We followed the recipe of ref 25 with the exception that 3 g/L glucose and ~100 μM $FeCl_3$ were used. The labeled amino acid was added only upon induction with IPTG. In producing the different selectively labeled samples, the amounts of labeled L-amino acid added per liter were Cys (50 mg), Gly (55 mg), Thr (120 mg), Ala (44 mg), and Leu (130 mg). The BL21(DE3)/pLysS strain was used throughout. Under these conditions, we experienced no scrambling of the label, even though auxotrophic strains were not employed.

Protein Reconstitution and Purification. The harvested cells were resuspended in a small volume of 50 mM Tris-HCl buffer, pH 8.5, and then lysed by a freeze−thaw cycle followed by sonication. Small amounts of solid DNase, RNase, and $MgCl_2$ were added at this stage. The protein was reconstituted as described previously,[45,64,66] with the exceptions that Triton and $Fe(NH_4)_2(SO_4)_2$ were not added and Tris-HCl buffer was used instead of potassium phosphate. Protease inhibitors were present at all stages of purification up to the last chromatography step: a protease inhibitor cocktail (either that from Sigma or Calbiochem) was added at ratios of 1:100 to the cell lysate and 1:10 000 to all subsequent purification buffers.

Following reconstitution, DE52 resin (Whatman Inc.; Newton, MA) was added directly to the diluted protein solution; the resin was washed with copious amounts of 50 mM Tris-HCl buffer, pH 7.5, loaded onto a column, washed with 50 mM Tris-HCl buffer, pH 7.5, containing 0.075 M NaCl, and then eluted with 50 mM Tris-HCl buffer, pH 7.5, containing 0.5 M NaCl. The protein was concentrated with an Amicon (Millipore; Billerica, MA) stirred cell and desalted on a G-10 column. The resulting solution was loaded onto another DE52 column and eluted with a 0.075−0.5 M NaCl linear gradient in 50 mM Tris-HCl buffer, pH 7.5. The protein-containing fraction was concentrated and desalted again with an Amicon stirred cell, loaded onto a Mono-Q column on a fast protein liquid chromatography (FPLC) system (Pharmacia; Piscataway, NJ), and eluted with a 0.0−1.0 M NaCl linear gradient in 20 mM Tris-HCl buffer, pH 7.5. The product was concentrated with an Amicon stirred cell and then purified on an FPLC system with a Sephacryl S-100 column equilibrated with 50 mM Tris-HCl buffer, pH 7.5, containing 0.15 M NaCl. Protein purity and concentration were determined by UV/visible absorption spectroscopy (HP 8452 diode-array spectrometer; Palo Alto, CA), on the basis of $A_{414}/A_{278} \geq 0.78$ and $\epsilon_{414} = 11\,000$ M^{-1} cm^{-1}, respectively.[64] Final yields of purified protein were typically 8−24 mg/L from M9 medium or 45−95 mg/L from SR medium.

NMR Sample Preparation. An Amicon stirred cell was used to concentrate the protein and to exchange the buffer to 50 mM potassium phosphate, pH 7.25, in 90% H_2O/10% $^{2}H_2O$ containing a small amount of DSS as the chemical shift standard. For some samples (vide infra), the exchange buffer was 50 mM pH* 7.25 potassium phosphate buffer in 99.8% $^{2}H_2O$ (where pH* indicates the uncorrected glass pH electrode meter reading); in those cases, the sample was then lyophilized and redissolved in "100%" $^{2}H_2O$. Protein concentrations were 1.0−6.1 mM, as indicated below, and the final pH (or pH*) was ~7.35. The protein samples were degassed by evacuation, back-filled with Ar, and then transferred in an anaerobic glovebox to either to 5 mm NMR tubes fitted with J Young valves (Wilmad; Buena, NJ) or to 10 mm diameter 1 mL volume NMR microcells (Wilmad) sealed with rubber septa.

NMR Spectroscopy. The sample temperature during NMR data acquisition was 20 °C. Experimental data sets and NMR equipment used to collect them were as follows: for 1D ^{1}H and 2D $^{1}H\{^{13}C\}$,

(63) Skjeldal, L.; Markley, J. L.; Coghlan, V. M.; Vickery, L. E. *Biochemistry* **1991**, *30*, 9078−9083.
(64) Xia, B.; Cheng, H.; Vandarian, V.; Reed, G. H.; Markley, J. L. *Biochemistry* **1996**, *35*, 9488−9495.
(65) Muchmore, D. C.; McIntosh, L. P.; Russell, C. B.; Anderson, D. E.; Dahlquist, F. W. *Methods Enzymol.* **1989**, *177*, 44−73.
(66) Cheng, H.; Xia, B.; Reed, G. H.; Markley, J. L. *Biochemistry* **1994**, *33*, 3155−3164.

Bruker DMX-400 and DMX-500 spectrometers with Bruker 5-mm TXI $^{1}H\{^{13}C,^{15}N\}$ triple-axis gradient probes; for 3D HC(C)H-COSY and (H)CCH-COSY, Bruker DMX-500 spectrometer with a Bruker 5-mm TXI probe; for 1D ^{13}C and 2D $^{13}C\{^{13}C\}$, Bruker DMX-500 spectrometer with a Bruker 5-mm QNP $^{13}C,^{31}P,^{19}F\{^{1}H\}$ switchable probe; for 1D ^{15}N, Bruker DMX-500 spectrometer with a Bruker 5-mm $X\{^{1}H\}$ tunable broadband probe; for 1D $^{13}C\{^{15}N\}$, Bruker DMX-600 spectrometer with a custom-made Bruker 10-mm $^{13}C\{^{1}H,^{15}N\}$ probe.

NMR Data Processing and Analysis. ^{1}H chemical shifts were referenced relative to the DSS internal standard (taken as 0 ppm), and ^{13}C and ^{15}N chemical shifts were referenced indirectly by use of chemical shift ratios.[67] The 1D spectra were processed with exponential line broadening. Some of the ^{13}C spectra and all of the ^{15}N spectra required baseline subtractions. Two- and three-dimensional spectra were processed with NMRPipe[68] and analyzed with Sparky.[69] The spectra were processed with cosine-bell window functions in all dimensions (except where noted) and extensively zero-filled prior to Fourier transformations.

3. Results and Analysis

Assignment Strategy Overview. The assignment strategy consists of six steps. First, the region of the protein distant from the [2Fe-2S] cluster is assigned by applying standard 2D and 3D NMR methods to a sample labeled uniformly with ^{13}C and ^{15}N. Second, the broadest ^{13}C resonances (primarily those arising from the Cys ligands) are identified and assigned to residue and atom type by selective ^{13}C labeling and 1D NMR spectroscopy. Third, the $^{13}C\{^{13}C\}$ CT-COSY experiment[29] is used to identify spin systems involving carbons near the paramagnetic center that are broadened but not shifted sufficiently to be resolved by 1D methods. Fourth, broadened backbone ^{15}N resonances are identified by residue type through selective ^{15}N labeling and 1D ^{15}N NMR spectroscopy. Fifth, 1D $^{13}C\{^{15}N\}$ difference decoupling is used to establish sequential connectivities and assignments resulting from prior identifications of C′ and N signals by residue type. Sixth, ^{1}H signals are assigned by paramagnetic-optimized 2D and 3D $^{1}H\{^{13}C\}$ experiments.

Traditional 2D and 3D Methods: Assignments of Diamagnetic Signals. The present work made use of previously reported assignments for the protein backbone (H^N, N, H^α, C^α, C′) and C^β carbons of $HuFd_{ox}$, which were obtained by traditional ^{1}H-detected 2D and 3D NMR experiments.[45] The assignments also incorporated the partial side-chain assignments for H10, H56, and H62 obtained earlier by ^{1}H-detected 1D and 2D NMR experiments.[61] We used 3D HC(C)H-COSY[70] and 2D $^{1}H\{^{13}C\}$ HSQC spectroscopy optimized for aliphatic and aromatic resonances to extend the earlier backbone assignments and to extend them to the side chains. This approach led to assignments to 87% of the signals from the ^{1}H and ^{13}C nuclei of residues external to 44−57 and 90−93 (residues in the cluster-ligating loops). No assignments were found for residues 17, 31, 43−57, 59, 79, 87, or 90−93, and those for S1 and S117 and T110 and T123 were ambiguous. Figure 1 shows a comparison of the diamagnetic assignments from our laboratory, both from the present and earlier[45,61] work, with those reported by others for $HuFd_{ox}$[62] and $BoFd_{ox}$.[55,56]

1D ^{1}H and ^{13}C NMR Spectra: Identification of the Signals from the Cys Ligands. By use of SuperWEFT[71] to suppress

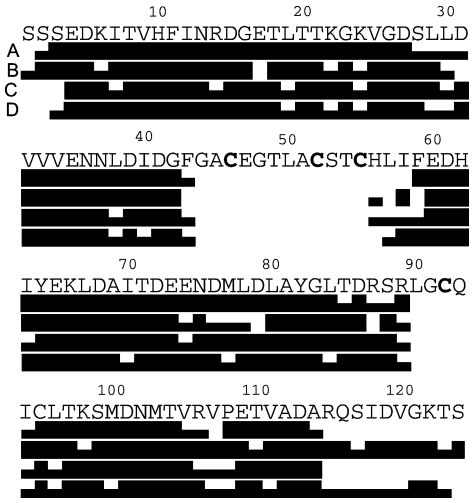

Figure 1. Diamagnetic sequential assignments obtained both from the present work and from our previously published studies of full-length $HuFd_{ox}$. The assignments are compared with those obtained by Pochapsky and co-workers for truncated $HuFd_{ox}$ and by Rüterjans and co-workers for $BoFd_{ox}$. Thick bars denote complete assignments, thin bars indicates incomplete or ambiguous assignments, and no bars indicate no assignment. (A) Full-length $HuFd_{ox}$, backbone assignments, from ref 45. (B) Full-length $HuFd_{ox}$, side-chain assignments from the present work, plus the His side-chain assignments from ref 61. (C) Truncated $HuFd_{ox}$, backbone and side-chain assignments, from ref 62. (D) Full-length $BoFd_{ox}$, backbone and side-chain assignments, from refs 55 and 56.

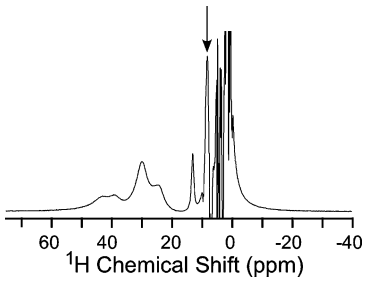

Figure 2. One-dimensional ^{1}H NMR spectrum acquired with SuperWEFT[71] of 4.0 mM $HuFd_{ox}$ in 100% $^{2}H_2O$, recorded on a Bruker DMX400 NMR spectrometer. The previously unreported broad peak at ∼8.4 ppm is indicated with an arrow. Complex points, 2048; spectral width, 150 ppm; acquisition time, 17.1 ms; recycle delay, 1.0 ms; SuperWEFT delay, 8.0 ms; number of scans, 2048; line broadening, 10.0 Hz.

the diamagnetic signals in the 1D ^{1}H NMR spectrum, we were able to identify a previously unreported broad ^{1}H peak at ∼8.4 ppm that integrates to ∼3 protons (Figure 2, Table 1). Figure 3 shows the 1D ^{13}C NMR spectra acquired by use of SuperWEFT of $HuFd_{ox}$ samples labeled uniformly with ^{13}C and ^{15}N (spectrum A), labeled selectively with [U-$^{13}C,^{15}N$]cysteine (spectrum B), and labeled selectively with [$^{13}C^\beta$]cysteine (spectrum C). In spectrum A, unresolved envelopes of peaks are seen in the usual carbonyl and aliphatic carbon regions. These correspond to resonances that are near enough to the [2Fe-2S] cluster to have shortened T_1 relaxation rates. Eight broad, hyperfine-shifted resonances were resolved in the 70−130 ppm region (labeled e−m). Spectrum B exhibits four resonances (a−d) in the C′ region and six broad resonances of one-carbon intensity and one of two-carbon intensity (e−h, k, m, and n). Spectrum C shows four resonances (i, k, m, and n). These data permitted the identification by atom type of the hyperfine-shifted carbon

(67) www.bmrb.wisc.edu.
(68) Delaglio, F.; Grzesiek, S.; Vuister, G. W.; Zhu, G.; Pfeifer, J.; Bax, A. *J. Biomol. NMR* **1995**, *6*, 277−293.
(69) www.cgl.ucsf.edu/home/sparky.
(70) Kay, L. E.; Ikura, M.; Bax, A. *J. Am. Chem. Soc.* **1990**, *112*, 888−889.
(71) Inubushi, T.; Becker, E. D. *J. Magn. Reson.* **1983**, *51*, 128−133.

Table 1. Assignments to Atom Type and Connectivity Information for the ^{1}H and ^{13}C Resonances of the Cys Ligands of Oxidized Human Ferredoxin at pH 7.35 and 20 °C

signal[a]	chemical shift (ppm)	atom type assignment	connectivity pattern
	13.10	$^1H^{\alpha}$	CysB
	8.61	$^1H^{\alpha}$	CysC
	8.17	$^1H^{\alpha}$	CysA
	8.12	$^1H^{\alpha}$	CysD
	34−42	$^1H^{\beta}$	
a	176.3	$^{13}C'$	CysA
b	175.4	$^{13}C'$	CysB
c	173.4	$^{13}C'$	CysC
d	171.7	$^{13}C'$	CysD
e	125.4	$^{13}C^{\alpha}$	CysB
f	110.6	$^{13}C^{\alpha}$	CysC
g	105.5	$^{13}C^{\alpha}$	CysA
h	102.7	$^{13}C^{\alpha}$	CysD
i	103.2	$^{13}C^{\beta}$	
k	89.5	$^{13}C^{\beta}$	
m	74.1	$^{13}C^{\beta}$	
n	58.8	$^{13}C^{\beta}$	

[a] Letters correspond to labels on ^{13}C resonances in Figure 3.

signals from the cysteines that ligate the two iron atoms: signals i, k, m, and n correspond to C^{β} carbons; e, f, g, and h to C^{α} carbons; and a, b, c, and d to C′ carbons (Table 1). Furthermore, Cys $C^{\alpha}-H^{\alpha}$ connectivities were determined from $^1H\{^{13}C\}$ difference decoupling (not shown, Table 1).[25,26] Of the hyperfine-shifted ^{13}C resonances seen in the spectrum of [U-^{13}C,^{15}N]-$HuFd_{ox}$ (Figure 3A), only signals j and l arise from non-Cys residues.

Two-Dimensional $^{13}C\{^{13}C\}$ NMR Spectra: ^{13}C Spin-System Identification for Residues in the [2Fe-2S] Cluster-Binding Loops. Figure 4 shows the region of the $^{13}C\{^{13}C\}$ CT-COSY spectrum of [U-^{13}C,^{15}N]-$HuFd_{ox}$ that contains cross-peaks from Ser and Thr. The results shown in Figure 4A,C were obtained with parameters appropriate for detection of diamagnetic resonances (τ_e = 10 ms, recycle time = 1.27 s); those shown in Figure 4B,D were obtained with parameters optimized for the detection of rapidly relaxing signals (τ_e = 5.6 ms, recycle time = 0.138 s). In the paramagnetic-optimized version (Figure 4B), three new $C^{\alpha}-C^{\beta}$ cross-peaks were observed, one in the Ser region and two in the Thr region; these are highlighted with black ovals in this and subsequent figures. The peak in the serine region is assigned to S53, the only serine expected to be paramagnetically broadened. The peaks in the threonine region, which also show $C^{\beta}-C^{\gamma}$ connectivities (Figure 4C,D), are assigned ambiguously to T49 and T54, the only two threonines in the cluster-binding loops.

The regions of the diamagnetic- and paramagnetic-optimized $^{13}C\{^{13}C\}$ CT-COSY spectra that contain glycine $C'-C^{\alpha}$ cross-peaks are shown in Figure S1A,B of the Supporting Information. Two previously unidentified cross-peaks were detected in the paramagnetic-optimized version, and one of these also appeared in the diamagnetic-optimized spectrum. These were assigned ambiguously to two of the three unassigned Gly residues (G44, G48, and G90).

Signals from the $C^{\delta 2}$ carbons of H10, H56, and H62 were reported previously,[61] and signals from the C^{β} carbons of H10 and H62 were assigned by ^{1}H-detected 3D experiments (vide supra). The diamagnetic- and paramagnetic-optimized $^{13}C\{^{13}C\}$ CT-COSY spectra each showed $C^{\gamma}-C^{\delta 2}$ cross-peaks from H10 and H62 (data not shown); the $C^{\gamma}-C^{\delta 2}$ cross-peak from H56 could not be resolved from the diagonal. The diamagnetic- and paramagnetic-optimized $^{13}C\{^{13}C\}$ CT-COSY spectra each showed the $C^{\beta}-C^{\gamma}$ cross-peaks expected for H10 and H62, plus a third cross-peak at 30.5−127.1 ppm that was assigned to the $C^{\beta}-C^{\gamma}$ of H56 (data not shown).

Figure 5 panels A (diamagnetic-optimized) and B (paramagnetic-optimized) show the region that contains $C^{\alpha}-C^{\beta}$ cross-peaks from several amino acid types, including Ala and Glu. Six of the cross-peaks in the paramagnetic-optimized spectrum were not detected in the ^{1}H-detected 3D spectra; of these, three were also not observed in the diamagnetic-optimized $^{13}C\{^{13}C\}$ CT-COSY spectrum. Two of the cross-peaks in the paramagnetic-optimized $^{13}C\{^{13}C\}$ CT-COSY spectrum have chemical shifts typical for Ala and are assigned ambiguously as A45 and A51. One is assigned to H56 on the basis of chemical shift. The cross-peak at 53.7−30.0 ppm showed further connectivity to a resonance at 38.6 ppm (data not shown), which in turn is connected to one at 179.4 ppm (see below). This spin system was assigned ambiguously to either E47 or Q93. The cross-peak at 57.3−27.1 ppm failed to show a clear additional connectivity owing to spectral overlap and was assigned ambiguously to either E47 or Q93 on the basis of its chemical shift. The cross-peak at 49.6−26.1 showed further connectivity to one at 53.6 ppm (Figure 4C,D) and was assigned ambiguously to one of the three unassigned leucines (L50, L57, or L90) on the basis of the chemical shifts of its spin system. The chemical shifts of this Leu spin system match those assigned by others to L57 in $BoFd_{ox}$ and truncated $HuFd_{ox}$;[55,56] therefore it is assigned to L57. Figure 5C,D shows an additional new cross-peak at 58.2−42.7 ppm. Although further connectivity information was unavailable, it was assigned ambiguously as L50 or L90 on the basis of its chemical shift.

Two additional cross-peaks were observed only in the paramagnetic-optimized spectrum: at 174.9−85.6 and 85.6−38.8 ppm (Figure S2A−D, Supporting Information). The resonance at 85.6 ppm corresponds to one of the two hyperfine-shifted resonances seen in the 1D ^{13}C NMR spectrum of [U-^{13}C,^{15}N]-$HuFd_{ox}$ (signal *l*). The only remaining unassigned residue that could generate such a spin system is Leu. Thus, these cross-peaks are assigned ambiguously to the $C'-C^{\alpha}$ and $C^{\alpha}-C^{\beta}$ of L50 or L90. No further connectivity could be detected. The one remaining hyperfine-shifted resonance (signal j at 95.1 ppm) is attributed to the one glycine whose resonances had not been identified previously.

In Figure 2 of ref 29, we reported the $^{13}C\{^{13}C\}$ CT-COSY spectrum of [^{13}C,^{15}N-Cys]-$HuFd_{ox}$ obtained with acquisition parameters that had been adjusted to allow detection of signals from nuclei that relax very rapidly. $C'-C^{\alpha}$ cross-peaks were observed for three of the four Cys that ligate the [2Fe-2S] cluster. These data, combined with the $^1H\{^{13}C\}$ difference decoupling data reported above, provide the $C'-C^{\alpha}-H^{\alpha}$ connectivities for each Cys (Table 1).

At least part of the ^{13}C spin system for every residue in the cluster-binding loops has now been identified. As described above, our strategy for obtaining sequential assignments of residues near the paramagnetic center relies on assigning both the C′ and N signals to residue type. At this point, three C′ resonances had been identified, two belonging to Gly spin systems and one to a Leu spin system. The remaining $C'-C^{\alpha}$ cross-peaks could not be identified owing to spectral overlap (Figure 6A).

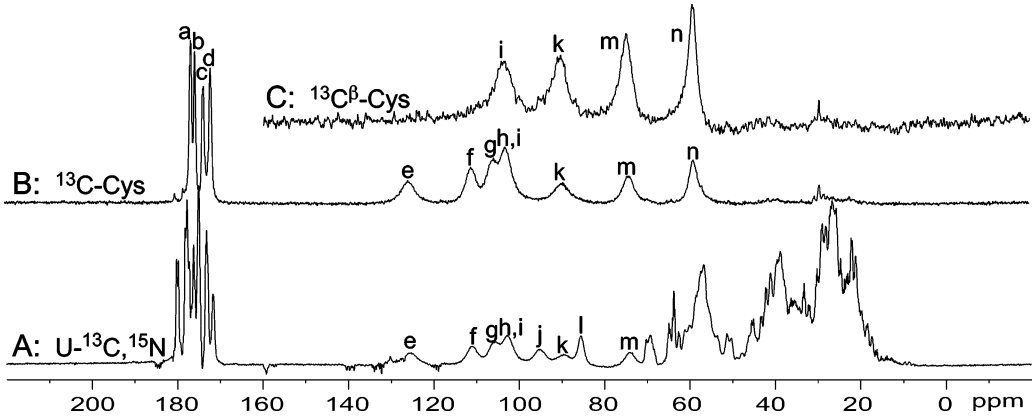

Figure 3. One-dimensional ^{13}C NMR spectra acquired with SuperWEFT[71] of $HuFd_{ox}$ in 90% H_2O/10% ^2H_2O, recorded on a Bruker DMX500 NMR spectrometer. Continuous ^{1}H decoupling was performed by use of a WALTZ16 composite pulse. (A) [U-^{13}C,^{15}N]-$HuFd_{ox}$, 4.4 mM. Complex points, 4096; spectral width, 390 ppm; acquisition time, 41.8 ms; recycle delay, 63.8 ms; SuperWEFT delay, 60.0 ms; number of scans, 42 000; line broadening, 1.0 Hz. (B) [^{13}C,^{15}N-Cys]-$HuFd_{ox}$, 6.1 mM. Number of scans, 40 000; line broadening, 5.0 Hz; other parameters the same as for spectrum A. (C) [$^{13}C^{\beta}$-Cys]-$HuFd_{ox}$, 1.0 mM. Recycle delay, 40.0 ms; SuperWEFT delay, 41.7 ms; number of scans, 84 000; line broadening, 5.0 Hz; other parameters the same as for spectrum A.

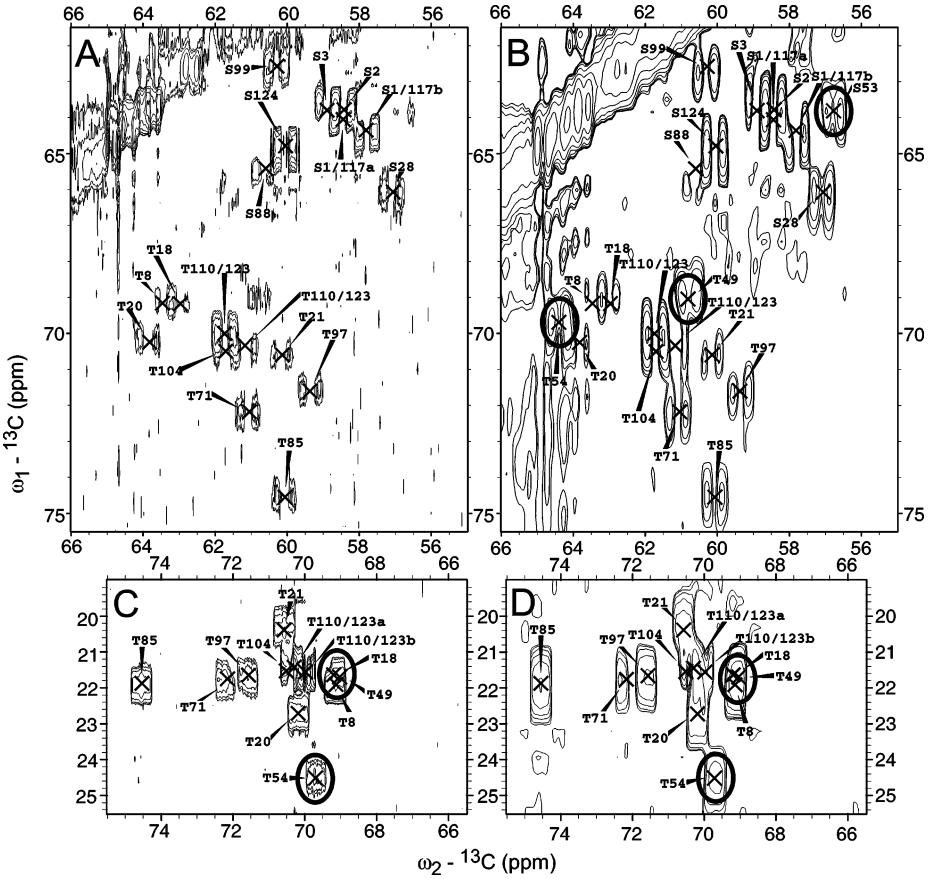

Figure 4. Comparison of the ^{13}C{^{13}C} CT-COSY spectrum of 4.4 mM [U-^{13}C,^{15}N]-$HuFd_{ox}$ in 90% H_2O/10% ^2H_2O, acquired on a Bruker DMX500 NMR spectrometer with parameters appropriate for a diamagnetic system (A, C) with the spectrum acquired with parameters optimized for rapidly relaxing signals (B, D). Spectra A and B contain the $C^{\alpha}-C^{\beta}$ cross-peaks of Ser and Thr residues, and spectra C and D contain the $C^{\beta}-C^{\gamma}$ cross-peaks of Thr residues. Phase-sensitive data were acquired with time-proportional phase incrementation (TPPI) and phased such that, in the direct dimension, diagonal peaks are in-phase absorptive and cross-peaks are antiphase dispersive. (A, C) Complex points, 460 (t_1) × 32 768 (t_2); spectral width, 184 (t_1) × 368 (t_2) ppm; acquisition time, 354 ms; τ_e, 10 ms; recycle delay, 1.0 s; number of scans, 96. (B, D) Complex points, 256 (t_1) × 4096 (t_2); spectral width, 184 (t_1) × 368 (t_2) ppm; acquisition time, 44.3 ms; τ_e, 5.6 ms; recycle delay, 90 ms; number of scans, 1600.

The problem of spectral overlap can be reduced by use of a relaxation-filtering element to suppress the signals from the much larger number of slowly relaxing diamagnetic signals. This was accomplished by use of the SuperWEFT (SW) pulse sequence element in front of the ^{13}C{^{13}C} CT-COSY experiment, in analogy to ^{1}H{^{1}H} WEFT-NOESY developed before.[72] This approach allowed the identification of the small number of signals from rapidly relaxing nuclei near the paramagnetic center. Figure 6B shows part of the $C'-C^{\alpha}$ region of the ^{13}C{^{13}C} SW-CT-COSY spectrum of [U-^{13}C,^{15}N]-$HuFd_{ox}$. Of

(72) Chen, Z. G.; deRopp, J. S.; Hernandez, G.; LaMar, G. N. *J. Am. Chem. Soc.* **1994**, *116*, 8772−8783.

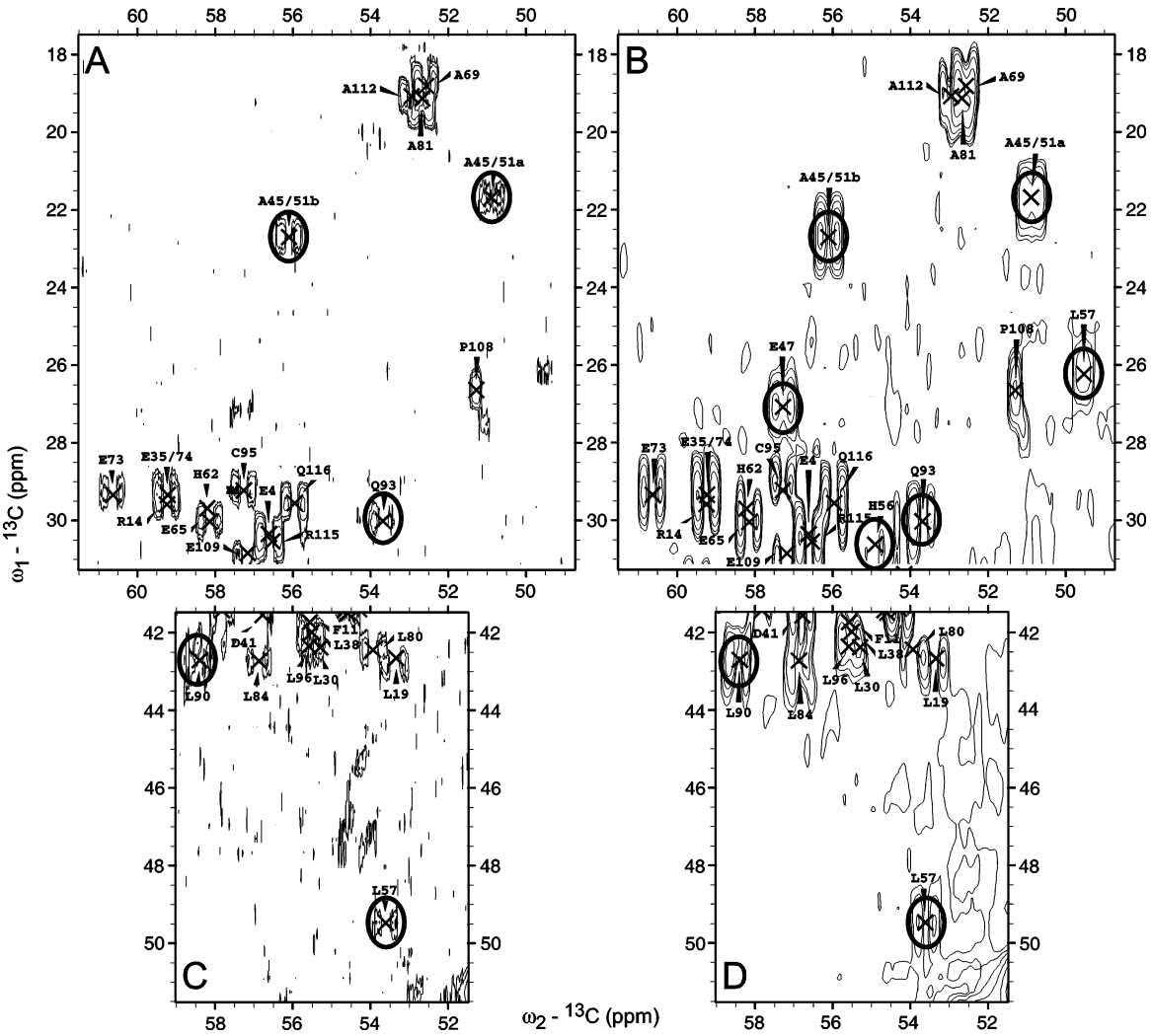

Figure 5. Comparison of other regions of the diamagnetic-optimized (A, C) and paramagnetic-optimized (B, D) $^{13}C\{^{13}C\}$ CT-COSY spectra of [U-^{13}C,^{15}N]-HuFd$_{ox}$. Spectra A and B contain the $C^{\alpha}-C^{\beta}$ cross-peaks of a number of residues, including Ala and Glu, and spectra C and D contain the $C^{\alpha}-C^{\beta}$ cross-peaks of Leu residues. Sample conditions and acquisition parameters are given in the caption to Figure 4.

the many overlapping peaks in Figure 6A, this approach permitted the resolution of 13 cross-peaks (nine of these are shown in Figure 6B). These signals include 12 of the 14 previously unidentified C′ resonances from residues in the cluster-binding loops, plus that from G42. Eleven of these signals could be added to existing spin systems for these residues. Since the C^{α} chemical shifts of L57 and Q93 are nearly identical, the cross-peak at 175.2−53.7 ppm was assigned ambiguously to one of these residues. The region of the spectrum in which cross-peaks from side-chain carbonyls are expected (Figure 6D) showed only one signal, which suggests that only one such side chain is sufficiently close to the [2Fe-2S] cluster to be rapidly relaxed. This signal is assigned ambiguously to the $C^{\gamma}-C^{\delta}$ of E47 or Q93.

One-Dimensional ^{15}N NMR Spectra: Identification of ^{15}N Resonances from Residues in the [2Fe-2S] Cluster-Binding Loops. Identification of amide ^{15}N signals by residue type was accomplished by selective ^{15}N labeling and 1D ^{15}N NMR (Figure 7). Figure 7A shows the 1D ^{15}N NMR spectrum of [U-^{15}N]-HuFd$_{ox}$. Diamagnetic amide ^{15}N signals appear at 110−130 ppm, and side-chain ^{15}N signals appear at ∼235, 170, 85, 70, and 35 ppm. In addition, nine hyperfine-shifted amide ^{15}N resonances were resolved: eight shifted to higher frequency, 132−181 ppm (a−h), and one shifted to lower frequency, 106 ppm (o). These have been assigned by incorporating [^{15}N]Cys, [^{15}N]Ala, [^{15}N]Leu, [^{15}N]Gly, or [^{15}N]Thr as shown in Figure 7B−F, respectively. In each case, 1−4 intense peaks were observed that correspond to signals from rapidly relaxing paramagnetic ^{15}N signals, along with a number of weak diamagnetic ^{15}N signals. Signals g−i and o are assigned ambiguously to the Cys ligands (C46/52/55/92); signals d and j are assigned ambiguously to A45/51; signals e, l, and m are assigned ambiguously to L30/50/90; signals a, k, and n are assigned ambiguously to G44/48/90; and signals b and f are assigned ambiguously to T49/54. From these data, 12 amide N nuclei from residues in the cluster-binding loops were identified by residue type, including all of the hyperfine-shifted ^{15}N signals with the exception of signal c.

One-Dimensional $^{13}C\{^{15}N\}$ NMR Spectra: Sequential Assignments of Residues in the [2Fe-2S] Cluster-Binding Loops. For nuclei with very fast relaxation rates, it is more difficult to determine $^{13}C'-^{15}N$ connectivities ($^1J_{CN}$ ∼14 Hz) than $^{13}C-^{13}C$ connectivities ($^1J_{CC}$ = 35−50 Hz). For this reason we used a 1D $^{13}C\{^{15}N\}$ difference decoupling experiment, rather than a 2D experiment, and we took advantage of the fact that nine ^{15}N signals are hyperfine-shifted and therefore could be

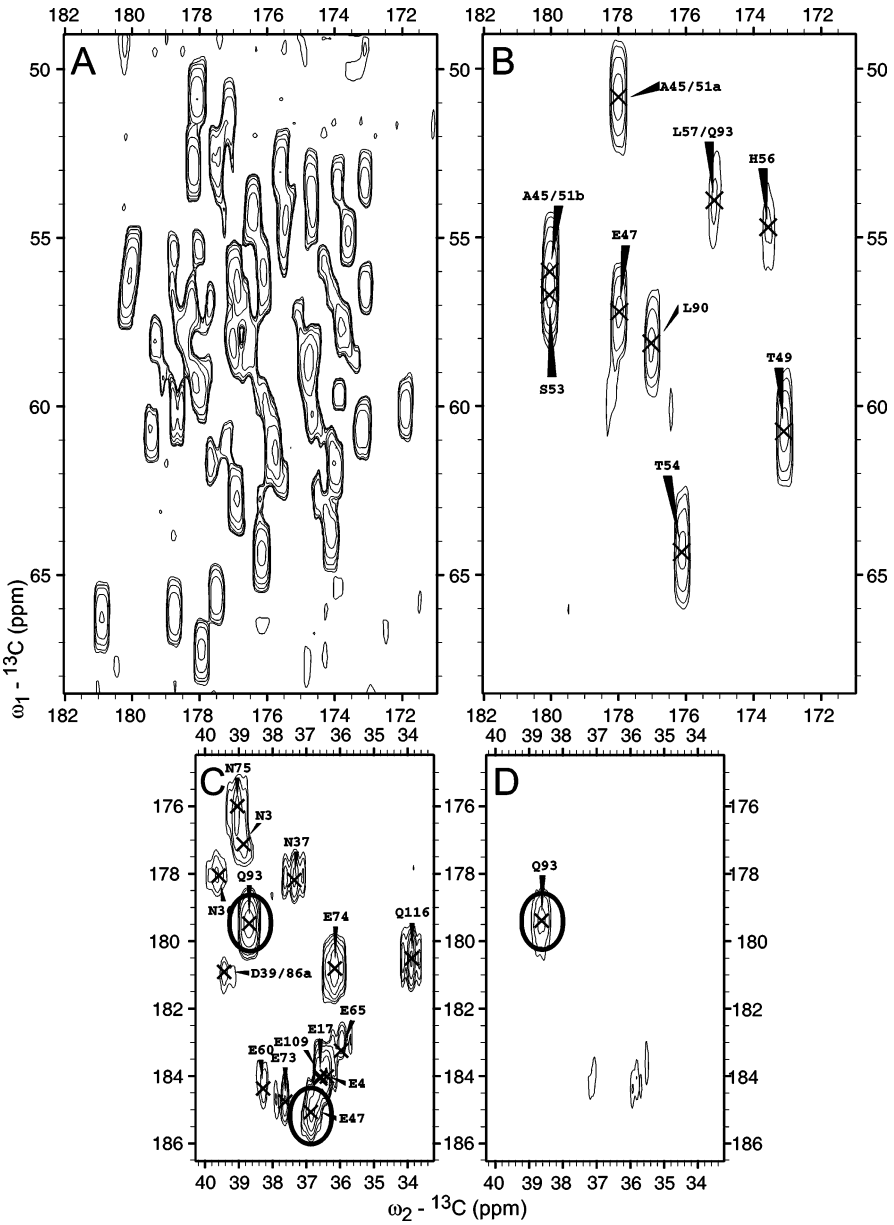

Figure 6. Comparison of the $^{13}C\{^{13}C\}$ CT-COSY spectrum of [U-^{13}C, ^{15}N]-HuFd$_{ox}$ without (A, C) and with (B, D) the SuperWEFT element for diamagnetic suppression. Spectra A and B contain the backbone C′−C$^{\alpha}$ cross-peaks, and spectra C and D contain some of the side-chain carbonyl cross-peaks. (A, C) Sample conditions, acquisition parameters, and phasing are given in the caption to Figure 4. (B) [U-^{13}C,^{15}N]-HuFd$_{ox}$, 4.0 mM in 100% $^{2}H_2O$. Complex points, 208 (t_1) × 4096 (t_2); spectral width, 190 (t_1) × 349 (t_2) ppm; acquisition time, 46.7 ms; SuperWEFT delay, 50 ms; τ_e, 5.0 ms; recycle delay, 53.3 ms; number of scans, 2080. (D) [U-^{13}C,^{15}N]-HuFd$_{ox}$, 4.0 mM in 100% $^{2}H_2O$. Complex points, 230 (t_1) × 8192 (t_2); spectral width, 190 (t_1) × 349 (t_2) ppm; acquisition time, 93.4 ms; τ_e, 5.0 ms; SuperWEFT delay, 150 ms; recycle delay, 200.0 ms; number of scans, 832.

decoupled selectively, even in U-^{13}C,^{15}N-labeled protein. The difference spectrum contains a single ^{13}C′ signal split by the scalar coupling from the $^{13}C^{\alpha}$.

The $^{13}C\{^{15}N\}$ difference decoupling spectra of [U-^{13}C,^{15}N]-HuFd$_{ox}$ are shown in Figure 8. Each spectrum is labeled with the ^{15}N signal that was decoupled. Decoupling of ^{15}N signals o, h, and g identified ^{13}C′ resonances at 180.0, 178.0, and 173.4 ppm, respectively. On the basis of assigned ^{13}C′ chemical shifts, these resonances are identified as arising from C46 ^{15}N−A45 ^{13}C′, C52 ^{15}N−A51 ^{13}C′, and C92 ^{15}N−G91 ^{13}C′. Owing to the redundancy in the sequence, the assignments of C46 ^{15}N−A45 ^{13}C′ and C52 ^{15}N−A51 ^{13}C′ are ambiguous; however, the assignment of C92 ^{15}N−G91 ^{13}C′ is unambiguous. The remaining Cys ^{15}N signal (i) is assigned to C55. Decoupling of ^{15}N signal e yielded a resonance at 173.1 ppm, which is assigned as L50 ^{15}N−T49 ^{13}C′. This provides unambiguous sequence-specific assignments for the carbon spin systems of T49 and T51. Decoupling of ^{15}N signal d yielded a resonance at 174.9 ppm, which is assigned to the A51 ^{15}N−L50 ^{13}C′ cross-peak. Decoupling of ^{15}N signal c yielded a resonance at 179.4 ppm. Although the ^{15}N assignment of signal c was not obtained by selective labeling, this ^{13}C′ chemical shift is consistent only with the spin system assigned to E47 or Q93. Thus, the carbon spin system is clearly that of Q93, and this connectivity can be assigned as Q93 $^{15}N^{\epsilon 2}$−Q93 $^{13}C^{\delta}$. The ^{13}C−^{13}C cross-peak at 57.3−27.1 ppm can be assigned then to E47. Decoupling of ^{15}N signal b yielded a resonance at 180.1 ppm, which is assigned to T54 ^{15}N−S53 ^{13}C′. Finally, decoupling of ^{15}N signal a yielded a resonance at 178.0 ppm, which is assigned to G48 ^{15}N−E47 ^{13}C′.

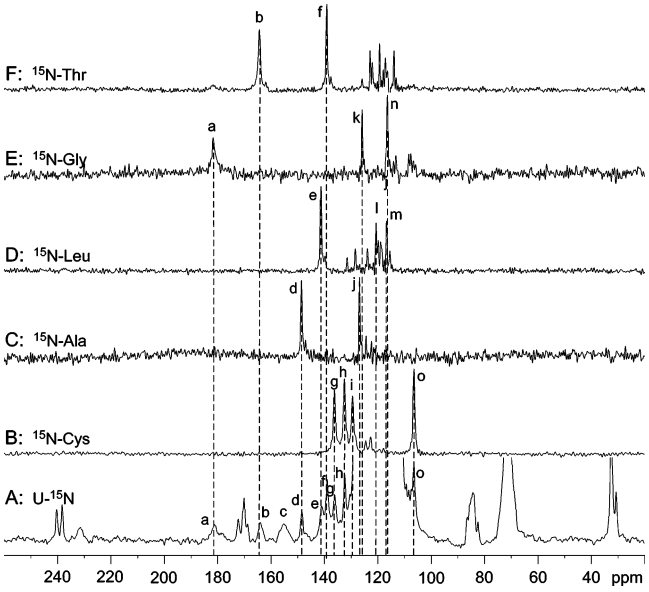

Figure 7. Comparison of the 1D ^{15}N NMR spectra of uniformly and selectively ^{15}N-labeled $HuFd_{ox}$ in 90% H_2O/10% ^2H_2O, recorded on a Bruker DMX500 NMR spectrometer. In spectra C−F, ^1H decoupling was applied during acquisition by use of a WALTZ16 composite pulse. (A) [U-^{15}N]-$HuFd_{ox}$, 2.2 mM. Complex points, 4096; spectral width, 401 ppm; acquisition time, 101 ms; recycle delay, 100.0 ms; number of scans, 96 000; line broadening, 25.0 Hz. (B) [^{13}C,^{15}N-Cys]-$HuFd_{ox}$, 6.1 mM. Complex points, 1024; spectral width, 401 ppm; acquisition time, 25.2 ms; recycle delay, 20.0 ms; number of scans, 720 000; line broadening, 5.0 Hz. (C) [^{15}NAla]-$HuFd_{ox}$, 5.5 mM. Complex points, 1024; spectral width, 299 ppm; acquisition time, 33.8 ms; recycle delay, 16.0 ms; number of scans, 610 000; line broadening, 2.5 Hz. (D) [^{15}N-Leu]-$HuFd_{ox}$, 5.4 mM. Number of scans, 320 000. (E) [^{15}N-Gly]-$HuFd_{ox}$, 4.4 mM. Number of scans, 320 000. (F) [^{15}N-Thr]-$HuFd_{ox}$, 4.7 mM. Number of scans, 650 000. All other acquisition parameters and line broadening are the same for spectra C−F.

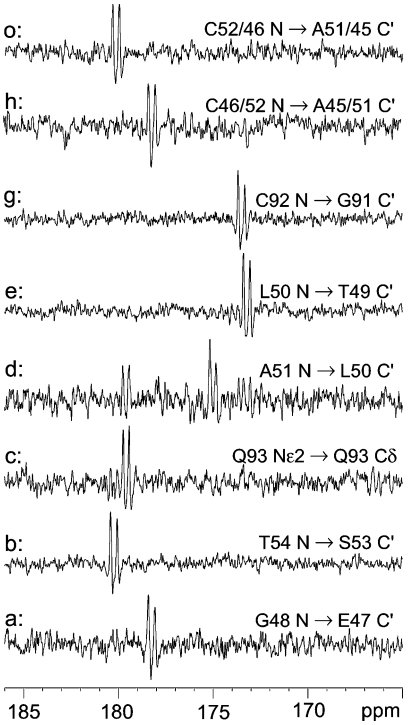

Figure 8. One-dimensional $^{13}C\{^{15}N\}$ difference decoupling NMR spectra of 4.2 mM [U-^{13}C,^{15}N]-$HuFd_{ox}$ in 90% H_2O/10% ^2H_2O, recorded on a Bruker DMX600 NMR spectrometer. The spectra are labeled according to the ^{15}N signal (Figure 7) that was selectively decoupled. The ^{15}N RF field strength was 177 Hz for a−d and 58 Hz for e, g, h, and o. Complex points, 2048; spectral width, 50 ppm; acquisition time, 135.2 ms; recycle delay, 90.0 ms; number of scans, 10 000 (except d, 20 000); line broadening, 6.0 Hz.

At this point, by a combination of selective and uniform labeling and 1D ^{13}C, 1D ^{15}N, 2D $^{13}C\{^{13}C\}$, and 1D $^{13}C\{^{15}N\}$ NMR experiments, we have obtained sequential assignments for nearly every residue in the cluster-binding loops. Few ambiguities remain. Definitive sequence-specific assignments for A45 and A51 are not possible with the method described here owing to the Ala−Cys redundancy inherent in the sequence. A solution to this would be to obtain $^{15}N-^{15}C^{\alpha}$ connectivity information. Attempts to do this by difference decoupling on U-^{13}C,^{15}N-labeled protein proved unsuccessful, likely because of the smaller scalar coupling (~9 Hz), and splitting of the $^{13}C^{\alpha}$ peak by both $^{13}C'$ and $^{13}C^{\beta}$. The Cys carbon spin systems were not assigned sequentially by this approach, because the amide ^{15}N nuclei of the adjacent residues (E47, S53, H56, and Q93) are not hyperfine-shifted. Although T49 ^{15}N is hyperfine-shifted, we have not obtained the T49 $^{15}N-$G48 $^{13}C'$ connectivity by difference decoupling and so cannot assign definitively G44 and G48. Nonetheless, given that G48 ^{15}N has a large hyperfine shift, it is reasonable to assume that its C^{α} would also be hyperfine-shifted. Thus the resonance at 95.1 ppm is tentatively assigned to G48. Table 2 contains the cumulative results, which include sequential assignments for at least one carbon atom in each residue of the cluster-binding loops except for the cysteines and two alanines.

^1H Assignments for Residues in the [2Fe-2S] Cluster-Binding Loops: Diamagnetic Suppression by Double Isotope Filtration. Once the sequence-specific assignments for ^{13}C and ^{15}N atoms in the residues of the cluster-binding loops were available, assignment of ^1H resonances was attempted. The identification of paramagnetic proton resonances presents multiple difficulties: (1) paramagnetic broadening is considerably greater for ^1H than for ^{13}C or ^{15}N, (2) the chemical shift dispersion for ^1H is much less than that for ^{13}C or ^{15}N, and (3) the filtration of diamagnetic resonances by a technique based upon saturation, such as SuperWEFT, is much less effective for ^1H than for ^{13}C because of the shorter T_1 relaxation rates of the proton.

A double isotope filter[73,74] (Figure 9) provided an adequate means of suppressing diamagnetic proton signals. The double isotope filter converts ^1H magnetization into multiple-quantum coherence, which is not observable. By repeating this with a slightly different delay, the whole range of aliphatic $^1H-^{13}C$ scalar couplings can be suppressed, regardless of relaxation rate. This filter is used typically for selective detection of a molecule at natural isotopic abundance bound to a U-^{13}C-labeled protein. It has been used in the SEA-TROSY experiment as an exchange filter to allow detection of solvent-exchangeable amide ^1H nuclei.[75] We have used the filter in a similar capacity, in which a delay after the double isotope filter allows fast relaxing resonances to recover *z*-magnetization. This is followed by a $^1H\{^{13}C\}$ heteronuclear single quantum coherence (HSQC) experiment that is optimized for fast-relaxing resonances by shortening the τ_3 delays in the pulse sequence (Figure 9A). Use of the double isotope filter as a paramagnetic relaxation editing

(73) Ogura, K.; Terasawa, H.; Inagaki, F. *J. Biomol. NMR* **1996**, *8*, 492−498.
(74) Breeze, A. L. *Prog. Nucl. Magn. Reson. Spectrosc.* **2000**, *36*, 323−372.
(75) Pellecchia, M.; Meininger, D.; Shen, A. L.; Jack, R.; Kasper, C. B.; Sem, D. S. *J. Am. Chem. Soc.* **2001**, *123*, 4633−4634.

Table 2. Assignments for the [2Fe-2S] Cluster-Binding Loops

	chemical shifts (ppm)						
residue	^{15}N	^{13}C′	^{13}C$^{\alpha}$	^{1}H$^{\alpha}$	^{13}C$^{\beta}$	^{1}H$^{\beta}$	other
G42	114.8[a]	174.0	46.1	4.11, 3.80			
F43	121.7	(178.0)[b]	59.4	4.60	40.9	(3.01, 2.01)[b]	^{13}C$^{\gamma}$, 139.0; ^{13}C$^{\delta}$, 133.3;[c] ^{1}H$^{\delta}$, 7.13; ^{13}C$^{\epsilon}$, 130.6; ^{1}H$^{\epsilon}$, 6.70
G44	*125.8/116.4*[d]	177.5	45.4	X[e]			
A45	126.8	*178.0/180.0*	*50.9/56.1*	*5.07/4.24*	*21.7/22.7*	*1.45/1.59*	
C46	*132.5/106.4*	f	f	f	f	f	
E47	X	178.0	57.3	X	27.1	*2.43, 2.27*	^{13}C$^{\gamma}$, *36.8*; ^{1}H$^{\gamma}$, *2.22*; ^{13}C$^{\delta}$, *185.0*
G48	181.1	X	95.1	X			
T49	139.0	173.1	60.8	X	69.0	4.57	^{13}C$^{\gamma}$, *21.7*; ^{1}H$^{\gamma}$, *1.12*
L50	140.8	174.9	85.6	X	38.8	X	X
A51	148.4	*180.0/178.0*	*56.1/50.9*	*4.24/5.07*	*22.7/21.7*	*1.59/1.45*	
C52	*106.4/132.5*	f	f	f	f	f	
S53	X	180.1	56.8	X	63.9	3.71	
T54	164.0	176.1	64.4	4.70	69.7	5.88	^{13}C$^{\gamma}$, *24.5*; ^{1}H$^{\gamma}$, *1.79*
C55	129.4	f	f	f	f	f	
H56	X	173.6	54.9	4.95	30.5	3.23	^{13}C$^{\gamma}$, *127.1*; ^{15}N$^{\delta1}$, 169.6;[g] ^{1}H$^{\delta1}$, 11.90; ^{13}C$^{\delta2}$, 127.2; ^{1}H$^{\delta2}$, 7.07; ^{13}C$^{\epsilon1}$, 137.8; ^{1}H$^{\epsilon1}$, 7.51; ^{15}N$^{\epsilon2}$, 238.2
L57	(128.3)[h]	175.2[i]	53.6	4.93	49.6	*1.73, 0.96*	^{13}C$^{\gamma}$, *26.1*; ^{1}H$^{\gamma}$, *2.38*; ^{13}C$^{\delta1}$, 28.7;[j] ^{1}H$^{\delta1}$, 1.01; ^{13}C$^{\delta2}$, 24.2; ^{1}H$^{\delta2}$, 1.04
I58	(119.8[b]/119.5[h])	(176.8[b]/177.1[h])	63.1	3.76	39.3	1.56	^{13}C$^{\gamma1}$, 28.7; ^{1}H$^{\gamma12}$, 1.62; ^{1}H$^{\gamma13}$, 1.02; ^{13}C$^{\gamma2}$, 16.9; ^{1}H$^{\gamma2}$, 0.91; ^{13}C$^{\delta}$, 14.6; ^{1}H$^{\delta}$, 0.91
R89	118.9	(176.8[b]/177.12[h])	52.83	4.875	34.08	2.028, 1.751	^{13}C$^{\gamma}$, 32.32
L90	*116.7/120.6*	177.9	58.21	4.58	42.70	X	X
G91	*116.4/125.8*	173.4	47.9	*4.53, 4.06*			
C92	136.2	f	f	f	f	f	
Q93	X	175.2[i]	53.7	3.6	30.1	*2.41, 1.44*	^{13}C$^{\gamma}$, *38.6*; ^{1}H$^{\gamma}$, *1.23*; ^{13}C$^{\delta}$, *179.4*; ^{15}N$^{\epsilon2}$, *155.0*
I94	X	174.1	57.9	4.25	37	2.35	^{13}C$^{\gamma1}$, 25.6; ^{1}H$^{\gamma12}$, 1.96; ^{1}H$^{\gamma13}$, 0.96; ^{13}C$^{\gamma2}$, 18.0; ^{1}H$^{\gamma2}$, 0.78; ^{13}C$^{\delta}$, 9.23; ^{1}H$^{\delta}$, 0.56

[a] Chemical shifts shown in Roman type are those reported herein or previously by us;[45,61] they were obtained by ^{1}H-detected diamagnetic assignment methods [3D backbone tracing, 3D H(C)CH-COSY, 2D aromatic ^{1}H{^{13}C} HSQC, and aliphatic ^{1}H{^{13}C} HSQC]. [b] Chemical shift assignments (in parentheses) for BoFd$_{ox}$ were determined by Rüterjans and co-workers by ^{1}H-detected methods for atoms not assigned by us.[55,56] [c] C−H cross-peaks for these were clearly observable in the diamagnetic 2D aromatic ^{1}H{^{13}C} HSQC; however, specific ^{13}C assignments relied heavily upon the 2D ^{13}C{^{13}C} CT-COSY data. [d] Chemical shifts shown in italic type were obtained as described here with the suite of paramagnetic 1D ^{15}N, 1D ^{13}C, 2D ^{13}C{^{13}C}, 1D ^{13}C{^{15}N},and 2D and 3D ^{1}H{^{13}C}experiments. [e] X = no assignments available. [f] See Table 1 for assignments and connectivity information; sequential assignments not available. [g] Chemical shifts for the H56 ring nuclei are those determined in this study; slightly different values were reported previously because of different sample conditions.[45] [h] Chemical shift assignments (in parentheses) for truncated HuFd$_{ox}$ were determined by Pochapsky and co-workers by ^{1}H-detected methods for atoms not assigned by us.[62] [i] Because the ^{13}C$^{\alpha}$ chemical shifts of L57 and Q93 are very nearly the same, this ^{13}C′ chemical shift could correspond to either residue. [j] The ^{13}C$^{\delta1}$−^{1}H$^{\delta1}$ and ^{13}C$^{\delta2}$−^{1}H$^{\delta2}$ cross-peaks were observed in the diamagnetic H(C)CH-COSY and ^{1}H{^{13}C} HSQC spectra but could not be assigned without the ^{13}C{^{13}C} CT-COSY and paramagnetic-optimized PRE-CT-(H)CCH-COSY data.

element (PRE) is superior to SuperWEFT when used in front of a paramagnetic-optimized 1D ^{1}H{^{13}C}HSQC sequence (data not shown). It has the additional advantage that it is unaffected by differences in diamagnetic T_1 relaxation rates or by the choice of recycle time.

Figure 10 shows the ^{1}H{^{13}C}PRE-HSQC of [U-^{13}C,^{15}N]-HuFd$_{ox}$. Several broad resonances were resolved that were not observed with a diamagnetic ^{1}H{^{13}C}HSQC pulse sequence. The data led to assignments of ^{1}H resonances from residues T49, S53, T54, and G91. Overlap precluded the identification of ^{1}H−^{13}C cross-peaks from other residues in the cluster-binding loops.

The problem of spectral overlap was solved by extending the experiment into a third dimension through use of a 3D constant-time (H)CCH-COSY. Because of the $1/\gamma_N^2$ dependence of paramagnetic relaxation, the limiting step in ^{1}H-detected NMR experiments is transfer of magnetization to and from the ^{13}C nucleus. An additional magnetization transfer step to the adjacent ^{13}C could be incorporated readily because transverse ^{13}C magnetization decays relatively slowly. A published CT-(H)CCH-COSY experiment developed for diamagnetic proteins[76] served as the starting point. Required modifications to develop a useful PRE-CT-(H)CCH-COSY experiment included the reduction of the number of gradients, replacement of sensitivity enhancement and echo−antiecho quadrature detection in the second ^{13}C dimension with quadrature detection by States-TPPI, and time-proportional phase incrementation (TPPI), and the addition of the PRE relaxation filter at the beginning of the sequence (Figure 9B). Figure 11 shows strip plots of data for several residues in the cluster-binding loops of [U-^{13}C,^{15}N]-HuFd$_{ox}$ obtained by PRE-CT-(H)CCH-COSY. Complete ^{1}H and^{13}C aliphatic side-chain connectivity was obtained for T54, A45/51, and H56. Additional connectivity information extended the spin systems of E47 to C$^{\gamma}$−H$^{\gamma}$ and L57 to H$^{\gamma}$−C$^{\gamma}$−C$^{\delta1}$−C$^{\delta2}$. The corresponding C$^{\delta1}$−H$^{\delta1}$ and C$^{\delta2}$−H$^{\delta2}$ cross-peaks were detected in the diamagnetic-optimized H(C)CCH-COSY and ^{1}H{^{13}C}HSQC spectra. Similarly, identification of the chemical shift of E47 ^{13}C$^{\gamma}$ led to the assignment of a cross-peak at 36.8−185.0 ppm in the ^{13}C{^{13}C} CT-COSY spectrum (Figure 6D) as E47 C$^{\gamma}$−C$^{\delta}$. However, for several other residues in the

(76) Gehring, K.; Ekiel, I. *J. Magn. Reson.* **1998**, *135*, 185−193.

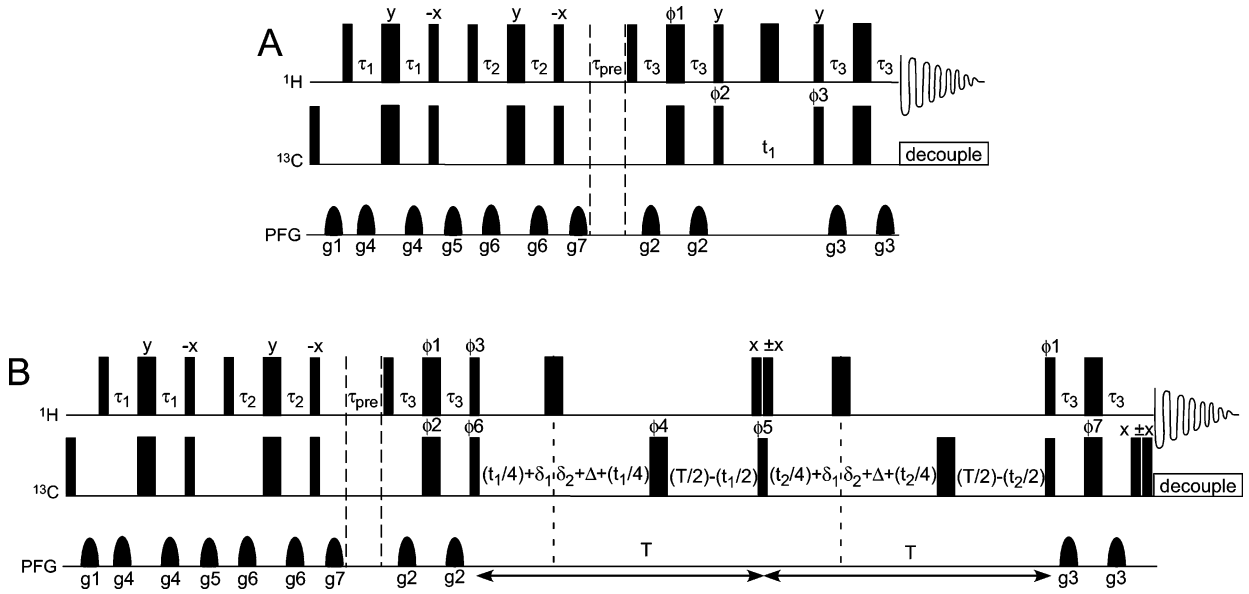

Figure 9. (A) $^{1}H\{^{13}C\}$ Paramagnetic relaxation edited (PRE-) HSQC pulse sequence. Narrow and thin bars represent 90° and 180° pulses, respectively. The dashed lines indicate the location of the relaxation editing delay (τ_{pre}); prior to it is the double isotope filter, and after it is an ordinary HSQC sequence. (B) PRE-CT-(H)CC-COSY pulse sequence. The longer dashed lines indicate the location of the relaxation editing delay (τ_{pre}); prior to it is the double isotope filter. The shorter dashed lines indicate the position of the ^{1}H 180° pulses relative to the delays discussed below. *T* is the constant time period and is typically ~7.8 ms for diamagnetic-optimized spectra, less for paramagnetic-optimized. t_1 and t_2 are the incremented delays for the first and second indirect ^{13}C dimensions, respectively. δ_1 is typically ~1.1 ms for diamagnetic-optimized spectra, less for paramagnetic-optimized. $\Delta = T/4$ and $\delta_2 = \Delta - \delta_1$. Detailed descriptions of the phase cycles, pulsed field gradients, and quadrature detection are provided in the Supporting Information.

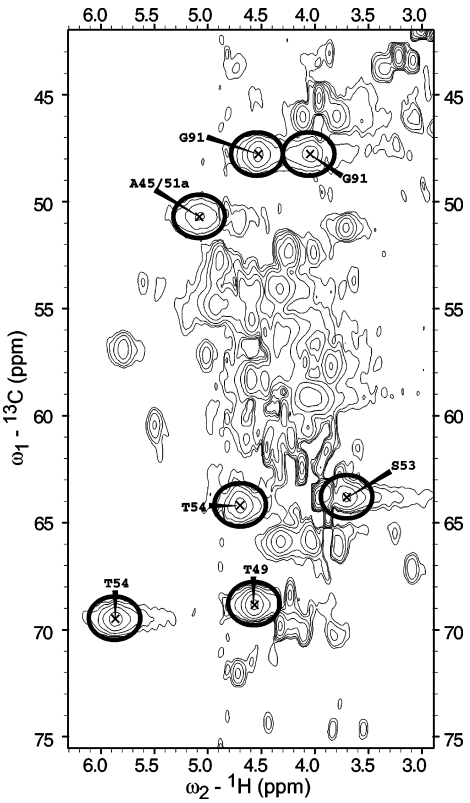

Figure 10. Portion of the $^{1}H\{^{13}C\}$ PRE-HSQC spectrum of 4.0 mM [U-^{13}C,^{15}N]-$HuFd_{ox}$ in 100% $^{2}H_2O$. Complex points, 204 (t_1) × 1024 (t_2); spectral width, 84 (t_1) × 26 (t_2) ppm; acquisition time, 49.2 ms; τ_1, 1.93 ms; τ_2, 1.77 ms; τ_{pre}, 8.00 ms; τ_3, 1.00 ms; recycle delay, 40.0 ms; number of scans, 240. ^{1}H decoupling was applied during acquisition by use of a GARP composite pulse. The spectrum was processed with a 45° shifted sine bell in both dimensions.

cluster-binding loops, such as S53, no cross-peaks could be found, even with the known ^{13}C chemical shifts. Thus, despite the greater sensitivity of ^{1}H detection, the faster relaxation rate of ^{1}H versus ^{13}C in a paramagnetic system limits the utility of even carefully designed paramagnetic-optimized ^{1}H-detected 2D and 3D experiments. The additional ^{1}H assignments that were obtained with these two experiments are included in Table 2.

3. Discussion

Assignment Summary. A combination of selective and uniform labeling and 1D ^{13}C, 1D ^{15}N, 2D $^{13}C\{^{13}C\}$, 1D $^{1}H\{^{13}C\}$, 1D $^{13}C\{^{15}N\}$, 2D $^{1}H\{^{13}C\}$, and 3D $^{1}H\{^{13}C\}$ NMR experiments have provided extensive spectral assignments to atoms in every residue in the cluster-binding loops of $HuFd_{ox}$. Overall, the signals from 88% of the carbons, 86% of the nitrogens, and 47% of the protons in the cluster-binding loops have been identified by residue and atom type.

The $^{1}H^{\alpha}$, $^{13}C^{\alpha}$, $^{13}C^{\beta}$, $^{13}C'$, and ^{15}N resonances of the Cys ligands have all been identified and assigned to atom type, and the $^{13}C'-^{13}C^{\alpha}-^{1}H^{\alpha}$ spin system of each Cys has been determined. Unambiguous sequence-specific assignments have been determined for the amide ^{15}N resonances of C55 and C92. For the remaining 14 residues in the cluster-binding loops, the $^{13}C'$ and side-chain assignments are complete for A45, A51, T54, H56, and G91, although the sequential assignments of the spin systems of A45 and A51 remain ambiguous. The side-chain assignments are complete for L57 and Q93, but only a single $^{13}C'$ has been identified that could belong to one of these residues. Complete carbon spin systems have been assigned for E47, T49, and S53 and tentatively for G44. C′ and partial side-chain assignments have been determined for L50 and L90. The ^{13}C resonance at 95.1 ppm has been assigned tentatively as G48 $^{13}C^{\alpha}$. For amide N resonances of these 14 residues, unambiguous sequential assignments have been obtained for A45, G48, T49, L50, A51, T54, H56, and L57, along with ambiguous assignments for G44/91, and L30/90. To our knowledge, these are

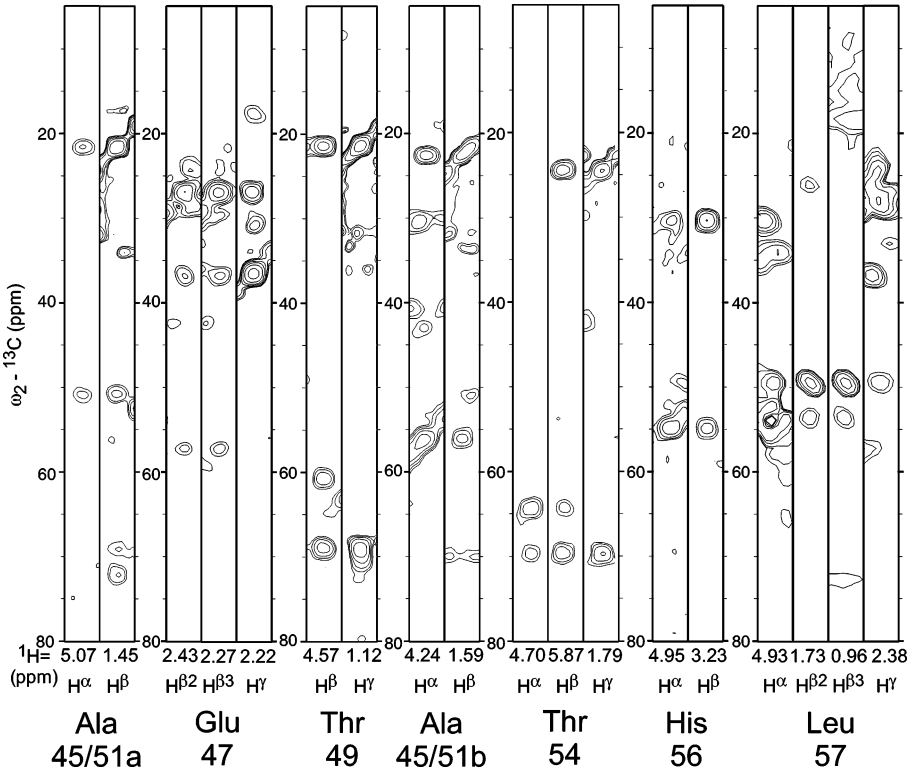

Figure 11. Selected strip plot from the PRE-CT-(H)CCH-COSY spectrum of 4.0 mM [U-^{13}C,^{15}N]-HuFd$_{ox}$ in 100% $^{2}H_2O$. Complex points, 120 (t_1) × 120 (t_2) × 1024 (t_3); spectral width, 84 (t_1) × 84 (t_2) × 28 (t_3) ppm; acquisition time, 36.0 ms; τ_1, 2.08 ms; τ_2, 1.70 ms; τ_{pre}, 8.00 ms; τ_3, 0.90 ms; *T*, 6.3 ms; δ_1, 0.55 ms; recycle delay, 54.0 ms; number of scans, 64. ^{13}C decoupling was applied during acquisition by use of a MPF7 composite pulse.[84] The strips for Leu57 were from a spectrum taken with the following differences in the acquisition parameters: complex points, 90 (t_1) × 90 (t_2) × 1024 (t_3); τ_1, 1.93 ms; τ_{pre}, 39.00 ms; recycle delay, 39.0 ms.

the most complete assignments available for any paramagnetic protein of comparable electronic relaxation rate.[77]

These assignments were obtained without the use of information from the crystal structure. Knowledge of hydrogen bonds to the FeS cluster and distances from the FeS cluster can be used as qualitative or semiquantitative tools for assignments in cases where such information is available. However, it is important that an assignment strategy be independent of such information for cases where crystallographic data are either unavailable or unreliable, such as when there are structural differences between the crystal and solution forms or between wild-type and mutant proteins.

Although the completeness of these assignments is unprecedented, the missing resonances deserve some comment. These fall chiefly into three categories.

(1) Amide ^{15}N resonances of E47, S53, H56, and Q93. As discussed above, these signals are not hyperfine-shifted and therefore would not be identified by our assignment strategy without additional selective labeling.

(2) Amide ^{1}H resonances of G44−H56 and G91−Q93 and $^{1}H^{\epsilon}$ resonances of Q93. These are predicted to be among the closest hydrogens to the [2Fe-2S] cluster: 3.54−6.56 Å from the Fe−Fe midpoint, based upon the crystal structure of truncated BoFd$_{ox}$.[40] For comparison, the T54 $^{1}H^{\beta}$, which is 6.83 Å from the Fe−Fe midpoint, has a line width (full width at half-height) of 81 Hz. Thus, it is unlikely that these resonances could ever be observed, much less assigned, with current methods.

(3) $^{1}H^{\alpha}$ resonances of G44, E47, G48, T49, and S53, $^{1}H^{\alpha}-^{1}H^{\gamma}$ resonances of L50, and $^{1}H^{\beta}-^{1}H^{\delta}$ resonances of L90. These are also very close to the [2Fe-2S] cluster: 3.63−6.93 Å from the Fe−Fe midpoint.

Applicability of the Methodology to Other Paramagnetic Proteins. These methods should increase the range of systems amenable to detailed NMR analyses, even in the absence of crystallographic data. Recent studies have demonstrated that one can obtain ^{1}H NMR data on Cu(II)-containing systems that were long thought inaccessible because of their slow electronic relaxation rates. Examples include the work of Canters and co-workers[78] and the work of Bertini, Vila, and co-workers.[79−81] However, only a few assignments have been obtained for signals from residues near the paramagnetic centers. The methods outlined here should be readily applicable to such systems and would greatly increase the amount of obtainable NMR data. In systems with less severe line broadening and larger pseudocontact shifts, the methods outlined here would be still easier to implement and could be combined readily with paramagnetic-optimized 2D ^{1}H NMR in order to increase the number and reliability of available assignments. Currently, the only alternative experimental approach for systems with slow electronic relaxation rates is extensive selective ^{13}C,^{15}N, or ^{2}H labeling of each amino acid type in the paramagnetic loops. This is true

(77) Extensive assignments have been made before for paramagnetic proteins with faster electronic relaxation, such as heme and [4Fe-4S] cluster proteins.

(78) Bubacco, L.; Salgado, J.; Tepper, A. W. J. W.; Vijgenboom, E.; Canters, G. W. *FEBS Lett.* **1999**, *442*, 215−220.
(79) Vila, A. J.; Ramirez, B. E.; Bilio, A. J. D.; Mizoguchi, T. J.; Richards, J. H.; Gray, H. B. *Inorg. Chem.* **1997**, *36*, 4567−4570.
(80) Bertini, I.; Ciurli, S.; Dikiy, A.; Gasanov, R.; Luchinat, C.; Martini, G.; Safarov, N. *J. Am. Chem. Soc.* **1999**, *121*, 2037−2046.
(81) Bertini, I.; Ciurli, S.; Dikiy, A.; Fernàndez, C. O.; Luchinat, C.; Safarov, N.; Shumilin, S.; Vila, A. J. *J. Am. Chem. Soc.* **2001**, *123*, 2405−2413.

regardless of whether NMR or EPR-based techniques such as electron−nuclear double resonance (ENDOR) and electron spin echo envelope modulation (ESEEM) are used. Sequential assignments would only be possible by carbonyl ^{13}C and amide ^{15}N double selective labeling, as has been done by Pochapsky and co-workers.[30−33] By comparison, the number of selectively labeled samples needed for the current approach is far lower. Given the good protein yields in SR media, the cost of materials was quite modest, although the labor required was high. The major limitation to our methodology has been the lower sensitivity of directly detected ^{13}C and ^{15}N NMR spectroscopy, which necessitates larger amounts of labeled protein. Improvements in NMR hardware, such as the recent introduction of liquid helium-cooled probes and preamplifiers, will certainly relax this limitation in the future.

Future Directions. With extensive assignments of the cluster-binding loops now available, the next step in determining a solution structure of $HuFd_{ox}$ that provides a clear picture of the [2Fe-2S] cluster is to obtain structural constraints for this region. Short-range distance constraints derived from the nuclear Overhauser effect (NOEs) provide the main input data for diamagnetic proteins. However, in the case of $HuFd_{ox}$, the very short ^1H T_1 rates strongly compete with the cross-relaxation that gives rise to the NOE. The paucity of ^1H assignments and the limited spectral dispersion of resonances in the cluster-binding loops would severely limit the utility of such data, assuming it could be obtained. Therefore, alternative structural constraints must be sought. Of these, the most obvious and frequently used are those that exploit the paramagnetism of the cluster: the electron−nuclear dipolar contribution to T_1 relaxation rates and pseudocontact shifts. We have already determined the T_1 relaxation rates for the identified ^{15}N resonances and the ^{13}C resonances of the Cys ligands. Although the remaining ^{13}C resonances of the cluster-binding loops cannot be resolved by 1D NMR, they can be readily resolved by 2D $^{13}C\{^{13}C\}$ experiments. Two-dimensional experiments for the measurement of T_1 relaxation rates have been developed,[82,83] and $^1H\{^1H\}$ versions have been applied in other paramagnetic proteins.[16,17] We are currently obtaining T_1 relaxation rate data for $HuFd_{ox}$ by use of 2D $^{13}C\{^{13}C\}$ experiments. Pseudocontact shifts are of little utility in the case of $HuFd_{ox}$. Because the magnetic susceptibility anisotropy in this system is small and a diamagnetic reference is unavailable (both oxidation states are paramagnetic, and no suitable substitutions are available for the iron atoms), the pseudocontact shifts are too small to be used reliably. Bertini and co-workers have discussed the value of different types of paramagnetism-based constraints and have shown that pseudocontact shifts are more effective than T_1 relaxation values as constraints. Therefore, there is a need to develop other types of geometric constraints for systems in which pseudocontact shifts cannot be used.

Acknowledgment. We thank Dr. Ronnie Frederick for advice on protein expression and Drs. Mark Anderson, Ed Mooberry, and Frits Abildgaard for spectrometer assistance. This work was supported by NIH Grant R01 GM58667; data were collected at the National Magnetic Resonance Facility at Madison, which has operating support from NIH Grant P41 RR02301. T.E.M. was supported by NIH postdoctoral fellowship F32 GM20497.

Supporting Information Available: Additional regions of the $^{13}C\{^{13}C\}$ CT-COSY spectra showing the relevant cross-peaks of residues in the cluster-binding loops and detailed descriptions of the phase cycles, pulsed field gradients, and quadrature detection for the PRE-HSQC and PRE-CT-(H)CC-COSY pulse sequences in Figure 9 (PDF). This information is available via the Internet at http://pubs.acs.org.

JA037077I

(82) Arseniev, A. S.; Sobol, A. G.; Bystrov, V. F. *J. Magn. Reson.* **1986**, *70*, 427−435.
(83) Kay, L. E.; Prestegard, J. H. *J. Magn. Reson.* **1988**, *77*, 599−605.
(84) Fujiwara, T.; Anai, T.; Kurihara, N.; Nagayama, K. *J. Magn. Reson. A* **1993**, *104*, 103−105.